ISSN 0916-5835

海洋音響学会誌

Vol. 51 No. 4 2024年10月 196

海洋音響学会

URL : https://www.masj.jp

THE JOURNAL OF THE MARINE ACOUSTICS SOCIETY OF JAPAN

Vol. 51 No. 4 October 2024

THE MARINE ACOUSTICS SOCIETY OF JAPAN

URL : https://www.masj.jp

Review

Development and Application of Advanced Science and Technology in Fisheries Acoustics

Dezhang CHU † *

Abstract:

The escalating impact of climate change, particularly since the turn of the century, has posed an increasingly formidable challenge to the global marine ecosystem. Effectively managing this ecosystem involves significant responsibilities for marine scientists, encompassing the tasks of monitoring, assessing, and researching the distribution of marine resources. Traditional fisheries surveys that employ trawl and net samplings, while effective, are both labor-intensive and time-consuming, rendering them inefficient. Since the mid to late 1930's, acoustic technologies have played a pivotal role in revolutionizing fisheries surveys, offering a more efficient means of conducting surveys for critical fish stocks worldwide. This paper provides an overview of the scientific and technological advancements achieved in fisheries acoustics over almost a century, with a particular focus on broadband and multibeam technologies. It also highlights the importance of theoretical modeling for understanding scattering by aquatic targets with complex shapes and varying material properties. To illustrate the benefits of employing these advanced scientific and technological approaches in fisheries research, some practical examples that emphasize on their advantages over traditional methods are provided.

1. Introduction

The mounting challenges of climate changes, especially in the 21st century, have significantly impacted the global marine ecosystem, presenting a formidable obstacle. Effective management of this ecosystem requires substantial responsibilities for marine scientists, including monitoring, assessing, and researching marine resource distribution. Although traditional fisheries surveys utilizing trawl and net samplings have been effective (Miller and Judkins, 1981; Frost and McCrone, 1974; Wiebe *et al*., 1976), they are labor-intensive and time-consuming, thus inefficient. Since the mid to late 1930's, acoustic technologies have played a crucial role in transforming fisheries surveys by providing a more efficient method for surveying critical fish stocks worldwide (Anon, 1934; Johns, 1934; Sund, 1935; Simmonds and MacLennan, 2005). Fisheries acoustics, a specialized field within marine science, utilizes sound waves to study aquatic organisms and their environment. It has become an essential tool for fisheries research owing to its non-invasive

† chu.dezhang@gmail.com

* Former affiliation: Northwest Fisheries Science Center, National Marine Fisheries Service, National Oceanic and Atmospheric Administration

nature and its capability to survey large areas efficiently (Kimura, 1929; Cushing, 1952; Anon, 1965, 1967; Simmonds and MacLennan, 2005). Over the past eight to nine decades numerous progresses in science and technology have been made in fisheries acoustics. This paper provides a brief overview of these progresses, including echosounder technologies, data processing and interpretation techniques, and the sampling platforms that carry the echosounder systems to conduct scientific research and fisheries surveys.

2. Science and technology advances in fisheries acoustics

The foundational technology used in fisheries acoustics involves emitting pulses of sound into the water and analyzing the echoes returned from underwater targets, such as fish and plankton. By applying empirical or theoretical acoustic scattering models, the biological information such as size, abundance, and biomass of these aquatic entities can be estimated and inferred (Medwin and Clay, 1998; Simmonds and MacLennan, 2005). The advancements in the science and technology of fisheries acoustics can be categorized into three main areas: data collection hardware—echosounders, data sampling platforms, and data processing or interpretation software.

Each of these components plays a vital role in the modern practice of fisheries acoustics, collectively enabling more precise and comprehensive studies of aquatic ecosystems, and is briefly described in the following subsections.

2.1 Echosounder systems

Since the introduction of sonar technologies into fisheries and zooplankton acoustics starting from as early as in the late 1920's to early 1930's of the 20th century, sonar or echosounder (downward-looking sonar) systems have evolved from the originally simple and primitive systems that primarily consisted of a single beam (channel) with a single narrow-band frequency to much advanced multi-beam and/or broadband systems (Kimura, 1929; Simmonds and MacLennan, 2005; Stanton, 2009; Korneliussen *et al*., 2009; Stanton *et al*., 2010; Chu, 2011). An online document from Simard, Kongsberg, a notable developer in this field, provides a comprehensive overview of this technology evolution along with the advances of their echosounder/sonar products (https://www.simrad.online/cat/scientific_all_a4_en_lores.pdf). Although this evolution has been a continuous process, several distinct milestones have significantly advanced fisheries acoustics, enabling it as an effective and efficient survey method for conducting large scale fisheries surveys (Fernandes *et al*., 2002). These developments not only allow for better survey capabilities but also enable a deeper understanding of marine ecosystems, contributing to more informed conservation and management decisions.

2.1.1 Qualitative to quantitative

Early applications of acoustics in fisheries were primarily qualitative (Johns, 1934; Anon, 1934; Sund, 1935), meaning the interpretations of echograms displayed on paper were only qualitative and were not able to provide quantitative biological information such as abundance and biomass based on robust scientific knowledge.

The shift from qualitative to quantitative analysis began to take shape in the mid-1960's. Dragesund and Olsen (1965) proposed a quantitative relationship between the received electric voltage and the fish abundance (number of fish) in an acoustically insonified volume, marking the beginning of using echo integration techniques for estimating fish population densities:

$$N \propto \int_T |v(t)| dt, \quad (1)$$

where $v(t)$ represents the received electric voltage, T is the transmit pulse duration, and N is the number of fish in the sample volume. The process of this accumulative sum of the received electric quantity is known as echo-integration, or echo-integrator. However, Scherbino and Truskanov (1966) discovered that the fish number density was more accurately correlated with the echo intensity rather than just the voltage, leading to the modified relationship:

$$N \propto \int_T |v(t)|^2 dt, \quad (2)$$

This change led to a more accurate relationship for assessing fish populations, establishing a more reliable foundation for quantifying fish abundance using acoustic data. This modification in echo-integration technique laid the foundation for correct abundance estimates in fisheries acoustics, enhancing its adoption in scientific and commercial fisheries management (Midttun and Nakken, 1968; Simmonds and MacLennan, 2005).

This improvement in echo-integration method enabled researchers and fishery managers to make more informed decisions based on robust acoustic data, facilitating better resource management and conservation practices. The evolution of these techniques illustrates the dynamic nature of technological advancements in marine science, particularly in how acoustic data is interpreted and used in ecological and fisheries research.

2.1.2 Analog to digital

The transition from analog to digital echosounders in the late 1960's and early 1970's marked a significant technological advancement in fisheries acoustics, driven by developments in electronics. This change enabled a more sophisticated handling of acoustic data, which was crucial for improving the accuracy and efficiency of marine studies.

Dowd's work in 1967 initiated this shift by showcasing the potentials of digital technologies in acoustic measurements. Further research by Dowd and others in 1970 highlighted that digital echo-integrators could achieve high correlation coefficients, greater than 0.90, for various pulse durations (Dowd *et al*., 1970), indicating reliable performance as shown in **Fig. 1**. The ability to record and store data digitally facilitated not only better data preservation and accuracy but also enhanced the capabilities for data processing. Technologies developed during this period allowed for more complex data manipulation, display, and analysis, significantly improving the quality and utility of acoustic data in marine research (Nickerson and Dowd, 1977; Brede, 1984).

This transition fundamentally changed how data was handled in marine acoustic surveys, setting the stage for the modern digital techniques used in today's marine research and fisheries management. The advancements in digital technology have continued to evolve, providing researchers with tools that are ever more precise and easier to use, enabling more detailed and comprehensive studies of marine environments.

2.1.3 Single frequency to multi-frequencies

Beginning in the early 1970's, development of the multi-frequency, or multiple discrete frequency, systems significantly strengthened scientists' ability to identify and classify aquatic objects due to complicated frequency dependence of these aquatic organisms (Holliday, 1971, 1977; Holliday *et al*., 1989; Jech and Michaels, 2006; Korneliussen *et al*., 2009). In the mid-1970's, dual-beam and split-beam were developed, which enhanced target detection capabilities. The dual-beam technology relied on the beampattern difference between the transducer aperture to locate the target, whereas the

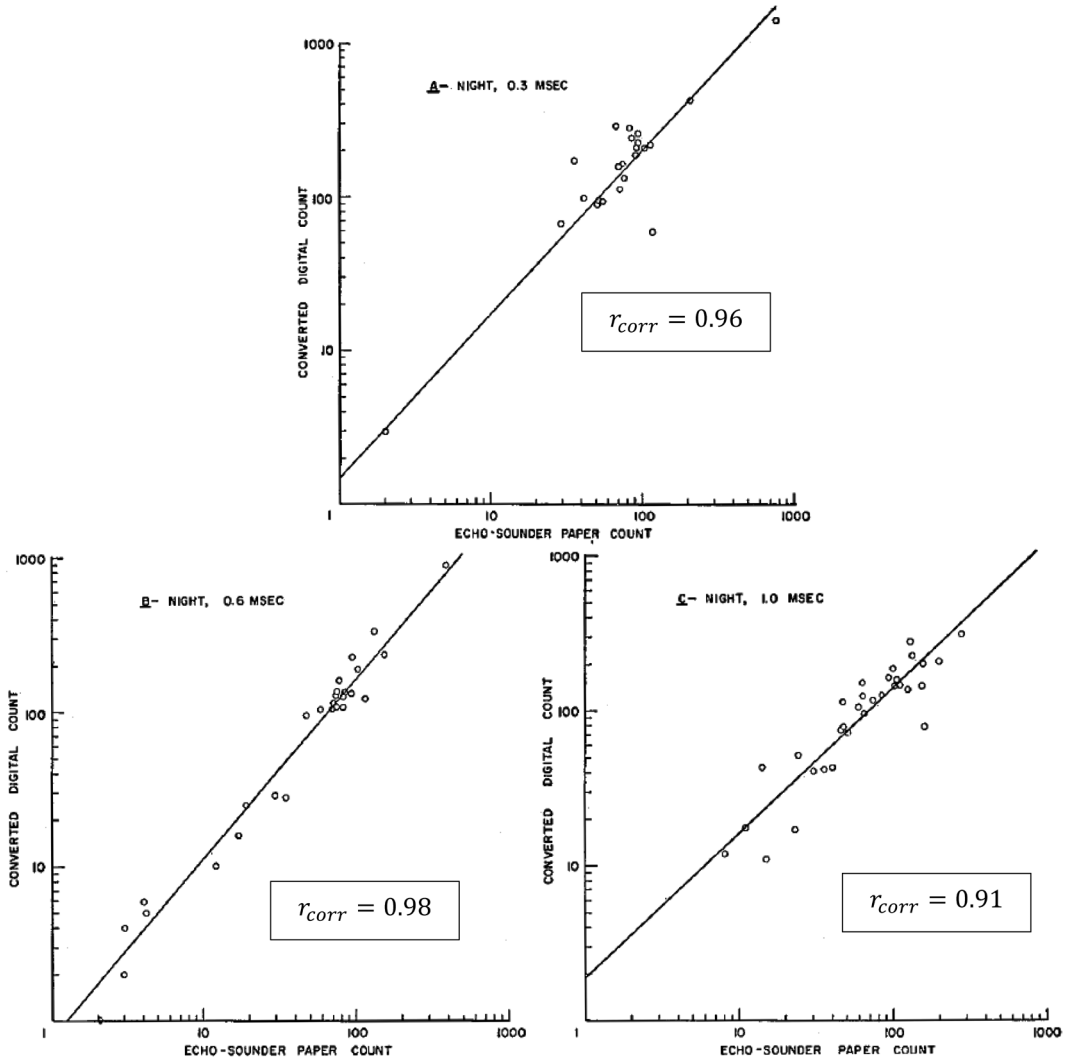

Fig. 1 Comparison between the analog and digital echo-integrators for different pulse durations. The echosounder frequency is 38 kHz. Figure is adapted from Dowd *et al*. (1970, with permission).

split-beam technology used the interferometry for target localization, to achieve more precise localization of an individual target within the field of view of the echosounders, resolving issues like angular ambiguity that were inherent in dual-beam systems (Ehrenberg, 1974; Hester, 1975; Foote, 1984). The latter included a system with four beams that could precisely determine the location of an individual target, with angular resolution proportional to the ratio of the transducer aperture to the acoustic wavelength.

Alongside the development of the multi-frequency technologies, echosounder linearity that relates the acoustic intensity and detected biological targets was further confirmed through convincing laboratory and *ex situ* observations (Foote, 1983). Concurrently, more accurate and practical calibration method and protocols were developed (Dragonette *et al*., 1981; Foote, 1982) and gained international acceptance (Demer *et al*., 2015).

2.1.4. Single beam to multibeam

The evolution from single beam to multibeam

echosounder systems marked a significant technological leap in marine acoustic surveying. While dual-beam and split-beam echosounders developed in the 1970's were capable of resolving accurately only one individual target at the same range within the beam. The true commercial multibeam acoustic systems, including down-looking echosounders such as Simrad ME70 and side-looking sonars such as Simrad MS70, were available not until the 1990's (Gerlotto *et al*., 1994, 1999; Mayer *et al*., 2002; Cochrane *et al*., 2003; Foote *et al*., 2005; Trenkel *et al*., 2008; Korneliussen *et al*., 2009; Cut *et al*., 2016). Most of the currently multibeam echosounders/sonars are pseudo 3D multi-beam systems, they can provide true 2D images in the athwartship plane for each ping (**Fig. 2**) and then forms a 3D volumetric image by compiling a series of pings along the ship track (Simrad, https://www.simrad.online/cat/scientific_all_a4_en_lores.pdf). These systems include Simard ME70, SM20 (formerly SM2000), and Reson Seabat 7000 and 8000 series.

The Simrad MS70, a true 3D multibeam system, is particularly notable for its array of 500 beams arranged in a 25×20 grid (**Fig. 3**). This setup allows for instantaneous, high-resolution imaging of marine life, including fish and zooplankton schools, providing critical data on their morphology and dynamics in real time (Korneliussen *et al*., 2009; Ona *et al*., 2009). Such advanced capabilities significantly enhance the capasibility of classification and characterization of aquatic species, offering profound insights into their behaviors and environments.

2.1.5 Narrow band to broadband

The transition from narrowband to broadband echosounder systems in fisheries acoustics provided a significant development in the field, enhancing the resolution and applicability of acoustic data. It is well established that the scattering or backscattering of aquatic organisms depends strongly on frequency, or more accurately on the dimensionless parameter, kd, where k is the acoustic wave number and d is the characteristic dimension (length, width, and height) of the aquatic object in question (Chu *et al*., 1993; Medwin and Clay, 1998; Stanton *et al*., 1998b; Lavery *et al*., 2010). This dimensionless parameter is proportional to the ratio of d to the wave length, i.e., $kd=2\pi(d/\lambda)\propto(d/\lambda)$ (Medwin and Clay, 1998). There is often a confusion between a broadband and a wideband system and the terms are frequently used interchangeably. However, to differentiate between the two, we define *a wideband echosounder* system as one that may contain a number of narrow-band frequencies but spans a wide frequency band. In contrast, *a broadband echosounder* system is characterized by its ability to transmit and receive acoustic signals that span a continuous frequency band, which is also wideband. A wideband system may also consist of either type of echosounder system, or a combination of both (as illustrated in **Fig. 4**).

Another aspect of interest is the definition of a broadband system, particularly through the use of a unique parameter known as a quality factor, Q. This factor commonly used to describe the frequency characteristics of an echosounder system. The quality factor is defined as the ratio of center frequency (f_c) to the 3-dB (or -3 dB) bandwidth ($BW_{3\,\mathrm{dB}}$). If the Q value of an echosounder system is greater than 10, it is classified as a narrow-band system. Conversely if the Q value is smaller than 3, it qualifies as a broadband system. If the Q value between 3 and 10, there is no consensus and may depend on specific applications or even uses' preference shown below:

$$Q=\frac{f_c}{BW_{3\,\mathrm{dB}}}\rightarrow\begin{cases}\geq 10 & \text{Narrowband}\\ \text{in between} & ??\\ \leq 3 & \text{Broadband}\end{cases} \tag{3}$$

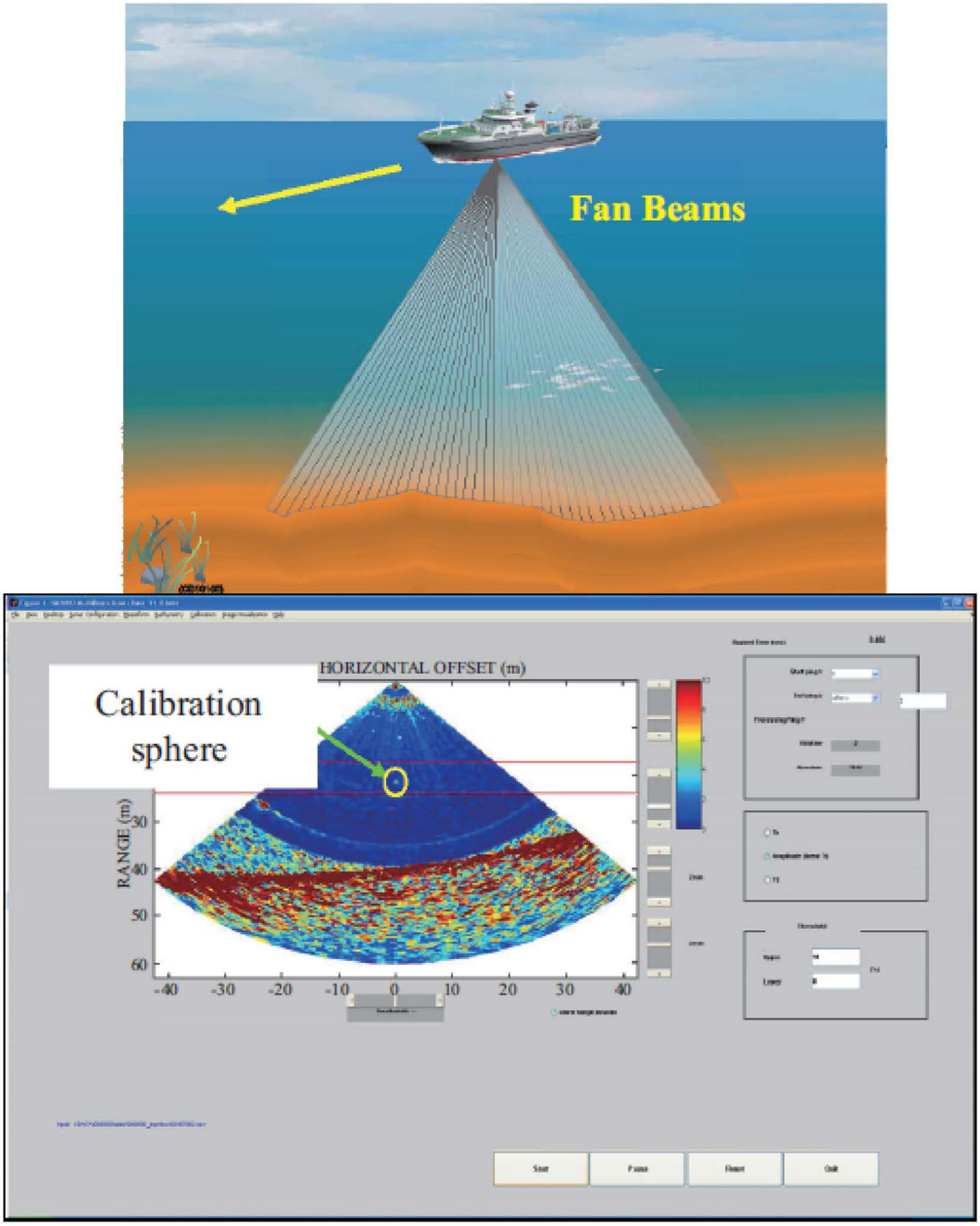

Fig. 2 Illustration of a 2D multi-beam echosounder, Simrad ME70 (top), and a Simrad SM20 image display of one ping during a calibration (bottom), where the calibration sphere is an aluminum sphere with a diameter of 38 mm (Chu, 2011).

The advantages of broadband systems include their ability to provide a continuous wideband frequency coverage of the scattered acoustic signals (3-dB bandwidth), a higher signal to noise ratio ($\propto T\,BW_{3\,\mathrm{dB}}^{-1}$, where T is pulse duration and $BW_{3\,\mathrm{dB}}$ is the system 3 dB bandwidth), and a higher temporal (spatial) resolution in the direction of wave propagation ($\propto BW_{3\,\mathrm{dB}}^{-1}$) (Chu and Stanton, 1998; Stanton, 2009; Stanton *et al*., 2010). The quality factor, Q, of the two commonly used broadband

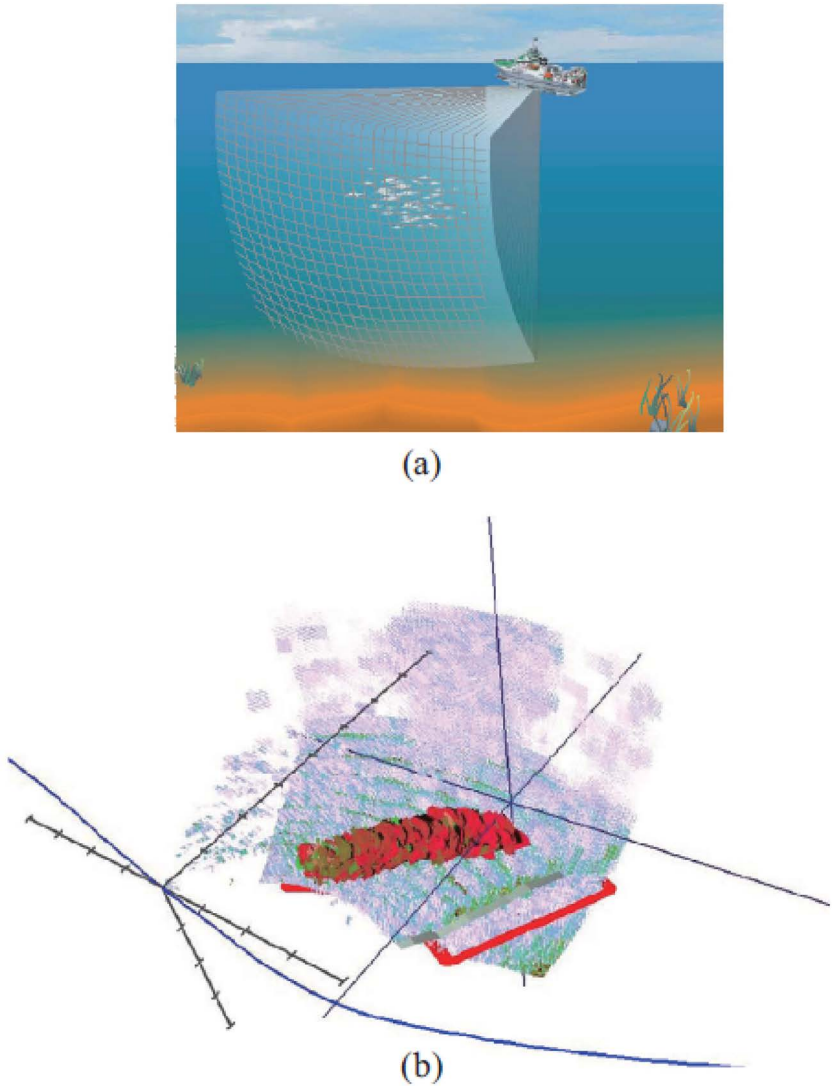

Fig. 3 (a) Illustration of a 3D multi-beam echosounder (Simrad MS70), (b) a herring school mapped by a single ping of the MS70 multibeam sonar system (Korneliussen, 2009; Chu, 2011).

echosounder systems in fisheries acoustics, Simrad EK80 and EdgeTech (towed echosounders), is listed in **Tables 1 and 2** for comparison. Table 1 also includes the Q parameters for the Simrad EK60 narrow band system.

An illustrative example of the temporal and spectral aspects of a broadband system is shown in **Fig. 5**. In this example, the transmit pulse duration is 1 ms, featuring an upsweep frequency from 50 to 90 kHz (f_c=70 kHz) over the entire pulse duration. The tapering function applied is a split Hanning window, covering about 10% of the pulse duration. The 3 dB bandwidth ($\Delta f_{3\,\mathrm{dB}}$) is a about 35 kHz, which is narrower than 40 kHz due to tapering, and the pulse temporal resolution is about 30 μs, slightly larger than the ideal temporal resolution (Δt=1/$\Delta f_{3\,\mathrm{dB}}$)=28.6 μs).

This shift from narrowband to broadband echosounder systems represents a significant technological advance in marine research, providing

researchers with more powerful tools for exploring and managing aquatic environments effectively.

2.2 Sampling platform

2.2.1 Ship-mounted echosounders

One important performance parameter of an echosounder is its signal-to-noise ratio (SNR). The SNR of an echosounder depends on many factors including both internal and external aspects. While the internal aspect is inherent to the echosounder and is normally fixed and stable for a period of time, the external aspect consists of environmental conditions and the sampling platform the echosounders are mounted to. Early fisheries acoustic surveys used hull-mounted echosounders to conduct fisheries acoustic surveys (Simmonds and MacLennan, 2005). It revolutionized fisheries survey by allowing scientists to efficiently and accurately estimate fish abundance and distribution in the water column. However, due to the direct coupling of the echosounders to the ship's hull, the mechanical and electrical interference from the ship itself resulted in a degraded quality of the recorded data and inferior performance of the echosounders.

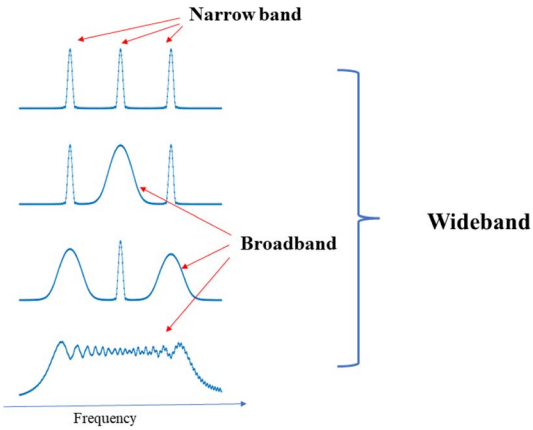

Fig. 4 Conceptual definitions of narrow-band, broadband and wideband echosounder systems.

Table 1 Quality parameters for Simrad EK60 and EK80 echosounders, where $Q=f_c/BW_{3\,\mathrm{dB}}$. For EK60 narrow-band echosounder: Using the minimum pulse duration to estimate the bandwidth with Hanning window of 100% tapering.

Nominal freq (kHz)	EK60		EK80			
	Min T (μs)	Est. Q	Center freq (kHz)	Freq range (kHz)	BW (kHz)	Est. Q
18	512	9	18	16–20	4	4.5
38	256	10	38	32–44	12	3.2
70	128	9	70	45–90	45	1.6
120	64	8	130	90–160	70	1.9
200	64	13	210	160–260	100	2.1
333	64	21	365	280–450	170	2.1

Table 2 Quality parameters for EdgeTech (https://www.edgetech.com) broadband echosounders (Stanton *et al*., 2005; Lavery *et al*., 2010).

Channel	Frequency band (kHz)	Center frequency (kHz)	Estimated Q
Shamu	1–12	6.5	0.6
424	4–24	14	0.7
Reson	45–105	75	1.3
Low	160–270	215	2.0
Medium	220–330	275	2.5
High–Low	330–470	400	2.9
High–High	450–590	520	3.7

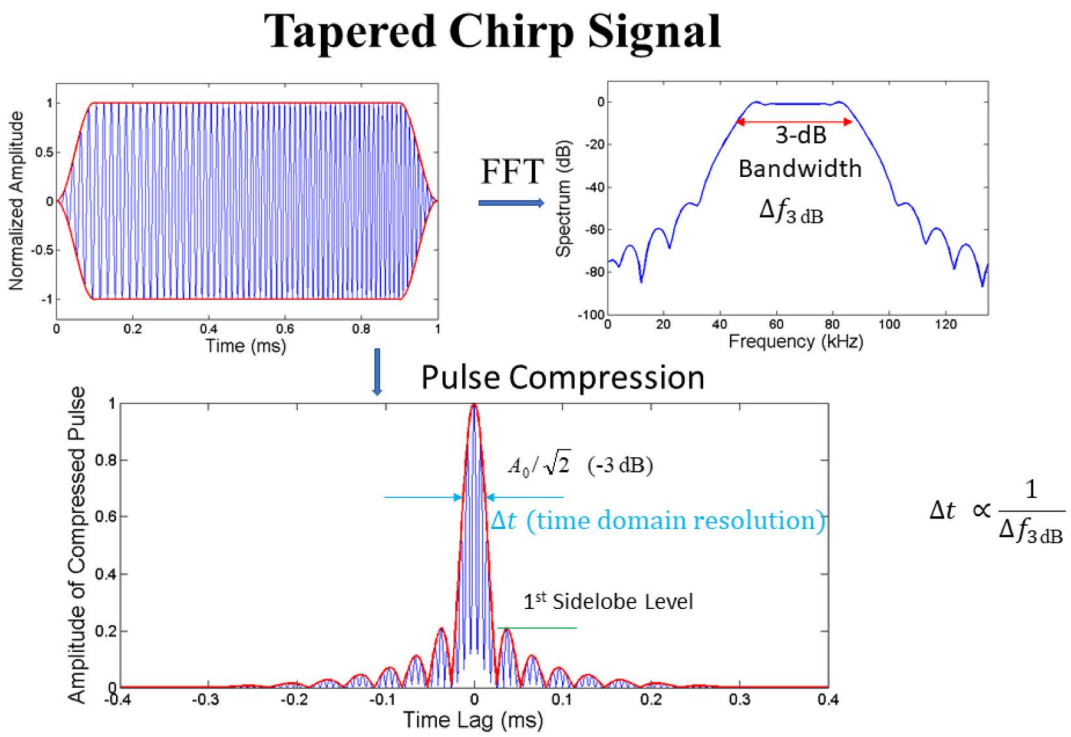

Fig. 5 Temporal and spectral characteristic of a broadband system.

To address these challenges, a significant improvement was made in the late 1960s and early 1970s with the introduction of echosounders mounted on a retractable centerboard. This design modification allowed the transducers to be indirectly coupled to the ship's hull, greatly reducing mechanical and electric cross-talk and enhancing the overall SNR of the acoustic data. However, while retractable centerboard mounting systems greatly improved data quality, they also introduced new challenges, such as increased drag when the ship was in motion. This increase in drag could lead to higher fuel consumption and, consequently, higher operational costs during surveys. Despite these drawbacks, the benefits of improved data accuracy and reliability often outweigh the increased costs, especially in comprehensive, large-scale fish stock assessments.

This development highlights the ongoing need to balance technological advancements with operational efficiency in marine research platforms.

2.2.2 Towed echosounders

Towed echosounders represent a dynamic and flexible approach to marine acoustic surveys, enabling researchers to collect high-resolution data from various depths and positions in the water column. Unlike ship-mounted systems, which are fixed to the vessel's hull, towed echosounders are deployed using a tow cable that includes electronic conducting wires, allowing for greater maneuverability and the ability to target specific depths and areas (Kloser, 1996; Dalen *et al*., 2003; Johnson and Smith 2019; Smith and Johnson, 2020). One of the advantages of a towed echosounder systems is that it can be deployed at any desirable depths hence achieve higher spatial (radial and angular) resolution since the spatial resolution is a function of range. This feature is very useful for exploring

the acoustical and biological characteristics of individual fish as well as fish schools. Another advantage of the towed systems is that the raw acoustic data can be displayed and processed in nearly real time, facilitating on-the-spot analyses and decision-making during survey operations.

A notable example of a specialized towed echosounder is the BIo-Optical Multi-frequency Acoustical and Physical Environmental Recorder II (BIOMAPER II). This system integrated the acoustic, bio-optical, and environmental data collection systems into a single towed sled (Wiebe *et al*., 2002). It was used to study a wide range of marine organisms including phytoplankton, zooplankton, and krill in the Gulf of Maine and the Antarctic Southern Ocean and provided a wide-angle view of microscopic sea life by measuring acoustic, bio-optical, and physical conditions simultaneously (Foote, 2001; Warren, 2001). With BIOMAPER II, broad-scale echosounder data, groundtruthed by bio-optical small-scale video and combined with environmental data, are capable of providing a complete picture of aquatic live animals in the water column. Such capabilities make towed echosounders invaluable tools for modern marine research, significantly enhancing our understanding of oceanic ecosystems.

2.2.3 Autonomous uncrewed vehicles

Autonomous uncrewed vehicles, including Autonomous underwater vehicles (AUVs) and uncrewed surface vehicles (USVs), have transformed the landscape of marine research by addressing some limitations inherent in traditional ship-mounted and towed echosounder systems. Since both types of data acquisition platforms require a mother-vessel to conduct data collection, the inevitable ship-induced noise not only reduce the SNR of the recorded acoustic data (ICES, 1995) but also alter behaviors of marine targets of interest (Goncharov *et al*., 1989; Brehmer *et al*., 2000). The development of these AUV/USV technologies not only enhances data collection efficiency but also significantly reduces the human and environmental footprint associated with marine surveys.

Developing AUVs, or Unmanned Underwater Vehicles (UUVs), offers a solution to overcome the limitations associated with ship-mounted and towed echosounders. The first autonomous underwater vehicles, the Self-Propelled Underwater Research Vehicle (SPURV), was developed as early as 1957 at the Applied Physics Laboratory, University of Washington for oceanographic research applications (Widditsch, 1973). SPURV was a battery-powered AUV equipped with a velocimeter (sound velocity), a quartz thermometer, and a thermistor-controlled Wien bridge oscillator (WBO), and later, a fluorometer.

While acoustic applications to map seafloor using either echosounders or sonars carried by AUVs were reported in the 1980's (Kosalos and Chayes 1983; Jarry, 1986; Tyce, 1986) and then have been extensively used internationally in marine geoscience (Wynn *et al*., 2014; Cutter *et al*., 2016), their applications to bioacoustics were not reported until 2010's.

AUVs, such as the REMUS [https://www.whoi.edu/what-we-do/explore/underwater-vehicles/auvs/remus/, **Fig. 6**(a)] (Moline *et al*., 2015), Autonomous Benthic Explorer (ABE), SeaBed developed at the Woods Hole Oceanographic Institution, Odyssey-class AUVs at MIT, and the D. Allan B at the Monterey Bay Aquarium Research Institute, represent some of the key developments in this technology. These vehicles are predominantly battery-powered and autonomous, capable of operating independently from human operators for the duration of their battery life, which typically lasts only a few hours. This limitation, along

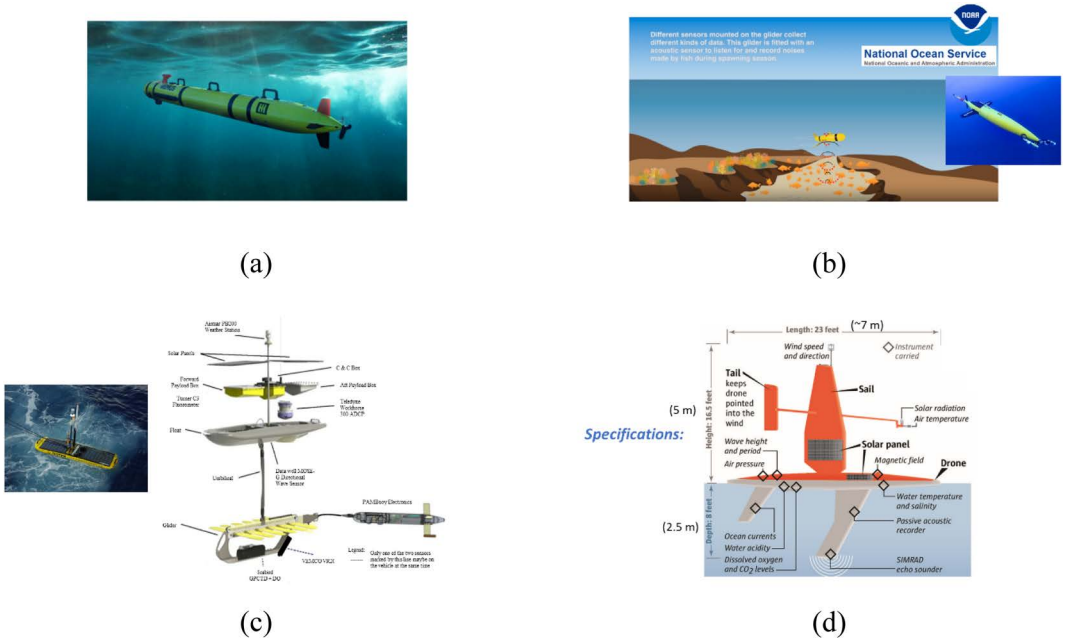

Fig. 6 Illustration of Autonomous Uncrewed Vehicles (AUVs): (a) REMUS (https://hii.com/what-we-do/capabilities/unmanned-systems/remus-uuvs/); (b) Ocean glider (https://oceanservice.noaa.gov/facts/ocean-gliders.html); (c) Wave Glider (https://www.liquid-robotics.com/; (d) Saildrone (https://www.seattletimes.com/seattle-news/science/saildrones-go-where-humans-cant-or-dont-want-to-to-study-the-worlds-oceans/).

with the need for deployment and recovery from a support ship, adds significant operational costs and logistical challenges (Moline *et al*., 2015).

Despite these challenges, the expansion of AUV capabilities has greatly enhanced our ability to explore and understand marine environments, offering tools that can reach areas that are otherwise inaccessible to human divers or larger manned vessels. The continued advancement in AUV technology promises further improvements in marine research, expanding our knowledge of the ocean's complex ecosystems and the life they contain.

Ocean gliders represent a type of Autonomous Underwater Vehicle (AUV) that harnesses natural energy sources to operate, utilizing a unique buoyancy-driven propulsion system [https://oceanservice.noaa.gov/facts/ocean-gliders.html, **Fig. 6**(b)]. These gliders adjust their buoyancy to sink or rise through the water, and their motion is converted into forward propulsion by wings attached to their bodies. This method of movement is highly energy-efficient, enabling ocean gliders to undertake extended missions lasting several months, often covering vast areas of the ocean (Benoit-Bird *et al*., 2018).

However, while these vehicles excel in energy efficiency for propulsion, they face limitations when it comes to powering onboard electronic data acquisition systems. The energy needs of these systems are entirely dependent on the batteries included in the AUV's payload. This dependency often constrains the operational capabilities of power-intensive instruments like echosounders, which are crucial for acoustic data acquisition. To manage energy consumption, ocean gliders may need to reduce the ping rate or shorten the operational duration of these systems, which could limit the depth and breadth of data collection during long missions.

Uncrewed Surface Vehicles (USVs) like Wave Gliders [https://www.liquid-robotics.com/wave-glider/how-it-works/, **Fig. 6**(c)] and Saildrones [https://www.saildrone.com/technology/vehicles, **Fig. 6**(d)]. utilize natural energy sources available at the water's surface to significantly enhance the efficiency and sustainability of maritime research operations, marking a significant advantage over other types of marine research vessels that rely on more traditional fossil energy sources.

Wave Gliders operate by harnessing the energy of ocean surface waves. They consist of two main parts: the float, which stays at the surface, and the sub, which is tethered below the float by a cable and moves vertically with the waves. This motion between the float and the sub is converted into forward thrust by the glider's unique design. The vertical movement of the sub in response to wave action allows Wave Gliders to traverse large distances without fuel, making them highly efficient for long-duration oceanographic missions.

Saildrones leverage wind energy for propulsion, using a sail attached to an unmanned autonomous vehicle. This setup allows them to navigate across oceans collecting data for months at a time. The sail provides the necessary power to move the drone and operate its instruments, making it ideal for various maritime research and observation tasks without direct human intervention.

One of the significant advantages of the USVs is that their main body remain on the water surface and can take advantage of the inexhaustible solar energy to charge their carried batteries through surface-mounted solar panels, or photovoltaic (PV), providing the electric power for the data collection electronic instruments including the echosounders that are essential for fisheries acoustics applications. Ideally, as long as the installed solar panels can convert sufficient solar energy to power all electronic data acquisition systems, these USVs can operate indefinitely at sea except for necessary maintenance. However, during cloudy days when the solar panels cannot provide adequate power, the USVs can remain on the surface for more days to charge the batteries. However, for systems like Wave Glider, noise generated by glider's operation can significantly interfere with echosounder systems so a towed system with a particular bouncy (about 6-m bellowed the sea surface), PAMBuoy, is needed for operating echosounders [**Fig. 6**(c)]. As a result, combination of the glider main body and a towed echosounder makes system's deployment and recovery very challenging, as well as making their operation more vulnerable to some unexpected event such as trawls from fishing vessels. In contrast, the echosounders that mounted on the keel of a Saildrone, about 5 feet below the main body, offer more reliable autonomous operation at sea, making it a more desirable for conducting fisheries acoustic surveys. A comparison of features among these different autonomous vehicles (AUVs, USVs) is provided in **Table 3**.

Both Wave Gliders and Saildrones represent innovative approaches to marine research, enabling the collection of vital environmental data while minimizing carbon footprints and operational costs. Their ability to harness natural energies contributes to their effectiveness in extended missions, particularly in remote or harsh environments where traditional vessel operations might be challenging or impractical. The evolution from traditional ship-based to autonomous survey methods marks a significant advancement in marine science, offering a way to conduct more respectful and less intrusive research in marine environments. These technologies continue to evolve, promising further improvements in how we study and interact with ocean ecosystems.

Table 3 Comparison of features among the different types of AUVs (USVs).

System	Survey speed	Sustainability	Payload	Deloy/recovery
Wind-Powered	medium	long	medium	easy
Wave-Powered	slow	long	medium	moderate
Gravity-Powered	slow	long	medium	easy
Battery-Powered	medium	short	high	easy

2.3 Scattering modeling by fish with and without swimbladder

2.3.1 Scattering by swimbladder-bearing fish

Since early 1930's, there has been significant progress in modeling scattering by swimbladder-bearing fish. Minnaert (1933) provided a formula to calculate the resonance frequency of a spherical bubble based on his "pulsation theory", which involved the principle of conservation of acoustic energy. An exact modal series solution was provided for a fluid sphere in the early 1950's by Anderson (1951) over an entire frequency band limited only to the computer's capability (convergence of the spherical Bessel functions at very high frequencies). Andreeva (1964) presented a resonance model that include an elastic wall around the gas-filled spherical gas bubble. A later publication by Feuillade and Nero (1998), extended Andreeva's work (1964), proposed a viscous-elastic model to describe the scattering. The model consisted of a spherical air bubble enclosed by an inner elastic shell representing the swimbladder wall, and then by an outer viscous shell representing the surrounding fish flesh. Using this viscous-elastic model, they obtained a good agreement between the theory and the measured data. This model was further modified to overcome its computational instability by replacing the Neumann functions with Hankel functions (Anson and Chivers, 1993) and validated by a good agreement between the theoretical predictions and those calculated using the finite element method (FEM) (Khodabandeloo *et al*., 2021), where nulls due to the interference among waves at some depths were reasonably predicted by the model.

A publication by Ainslie and Leighton (2011) provided an extensive review of scattering and extinction cross-sections, damping factors, and resonance frequencies of a spherical gas bubble in terms of the representative forms of the resonance scattering [Eqs. (1) and (2) in Ainslie and Leighton, 2011], where the resonance frequency and its radiate, viscous, and thermal damping were investigated.

Since most fish swimbladders are elongated and non-spherical, using prolate spheroids to approximate the geometric shape of fish swimbladders became a natural choice, especially for scattering near and below resonance frequency, which involves only non-directional breathing mode. A renowned work by Strasberg extended the Minnaert's resonance frequency formula for spherical bubbles to non-spherical spheroidal bubbles (Strasberg, 1953). In 1973, by applying Strasberg's formula of resonance frequency for spheroids, Weston presented a scattering model by a prolate spheroid as a function of frequency near or smaller than resonance frequency (Weston, 1973). His model included only the radiation damping. Love (1978) further developed a scattering model for a prolate spheroid with inclusion of thermal and viscous properties of fish swimbladder and flesh. At the same time, he corrected a typo in Weston's work for predicting the resonance frequency of a prolate spheroid (Love, 1978). However, since Love's work was primarily based on a spherical

bubble, his scattering function only considered the influence of bubble elongation on the resonance frequency not on the scattering amplitude. Nearly two decades later, Ye introduced a scattering model that accounted for the elongation effects on both resonance frequency, radiation damping, and the scattering amplitude (Ye, 1997). A resonance scattering model based on Ye's but including the viscous and thermal damping factors was proposed by Scoulding *et al*. (2015, 2022).

Except for the exact fluid sphere model and the viscous-elastic model, which is valid only for spherical gas bubbles and requires to solve a 10×10 linear equation system that involves Bessel functions of the first and second/third kinds (Feuillade and Nero, 1998; Khodabandeloo *et al*., 2021), all the previous resonance scattering models (Andreeva, 1964; Weston 1973; Love, 1978; Ye, 1997; Scoulding *et al*., 2015, 2022) are valid only for frequencies that are lower and around resonance frequency.

In this section, we propose a hybrid scattering model for fish with swimbladders that is valid in the resonance scattering, the geometric scattering regions, and extends to the ultimate asymptotic scattering level. Rather than pursuing an exact solution—which requires solving complicated equations and can be difficult to implement with adequate accuracy, especially for higher frequencies—we propose an approximate hybrid scattering model. This model is analytical and straightforward to implement, an essential attribute for solving inverse problems using a model-based iterative and/or Bayesian approach (Chu *et al*., 2016). In addition, each term in the analytical form of the scattering model has a clear physical and mathematical significance. The geometry of the scattering by an ellipsoid is depicted in Cartesian coordinates in **Fig. 7**. The resonance scattering for a prolate spheroid, a special case of an ellipsoid when $a=b$,

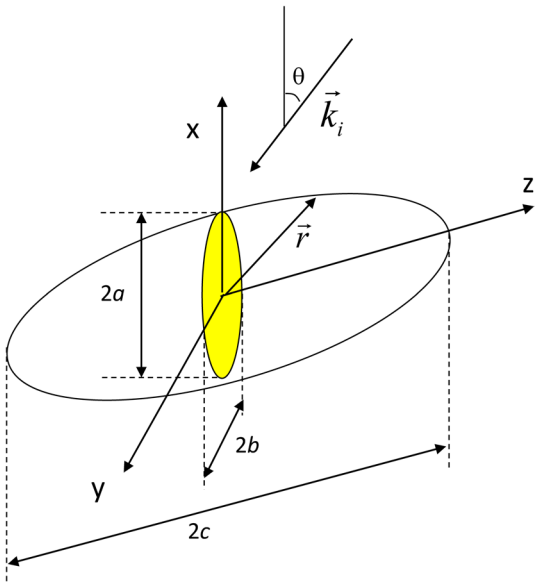

Fig. 7 Geometry of an ellipsoid in a Cartesian coordinate system.

is based on the model proposed by Ye (1997) but presented here in a slightly different form:

$$\sigma_{bs_0}^{res}(ka_{esr}) = \frac{a_{esr}^2 F_{spheroid}^2}{\left[\left(\frac{\omega_{spheroid}}{\omega}\right)^2 - 1\right]^2 + k^2 a_{esr}^2 F_{spheroid}^2}, \tag{4}$$

where a_{esr} is the equivalent spherical radius of a prolate spheroid, and

$$\omega_{spheroid} = \omega_{0_{esr}} F_{spheroid}^{1/2}, \tag{5a}$$

and the resonance frequency for a sphere of an equal volume of the prolate spheroid,

$$\omega_{0_{esr}} = \frac{1}{a_{esr}} \sqrt{\frac{3\gamma P_e}{\rho_w}} \tag{5b}$$

with an elongation factor:

$$F_{spheroid}^{1/2} = 2^{\frac{1}{2}} e_{ac}^{-\frac{1}{3}} \left(1 - e_{ac}^2\right)^{\frac{1}{4}} \left[\ln\left(\frac{1+\sqrt{1-e_{ac}^2}}{1-\sqrt{1-e_{ac}^2}}\right)\right]^{-\frac{1}{2}} \tag{5c}$$

where $e_{ac}=a/c<1$ is the aspect ratio, the ratio of semi-minor to semi-major axis. Note that it is easy to verify that the elongation effect of prolate spheroids reduces to unity for the case of a sphere, i.e., $F_{spheroid}=1$ for $e_{ac}=1$. It is obvious that the effects of the elongation of prolate spheroids not only on the resonance frequency (Weston, 1973; Love, 1978), but also on the damping (denominator) and amplitude (numerator) as well (Ye, 1997). This model ignores the viscous and thermal damping, as well as the potential interactions among the incident and scattered waves from different part of the fish swimbladder and the body at higher frequencies as investigated and reported by Khodabandeloo *et al*. (2021). It was also demonstrated that the thermal and viscous damping due to surface tension at the swimbladder/fish body interface, and the viscosity of the fish body played negligible effect on the backscattering by swimbladder fish as long as the frequency is outside a narrow band around the resonance frequency (Scoulding *et al*., 2015, 2022).

To account for orientation dependence of the scattering, a Sinc function can be introduced as in Stanton (1989) and Scoulding *et al*. (2015):

$$\Theta(\theta)=\frac{\sin(kc\sin\theta)}{kc\sin\theta}, \tag{6}$$

where θ is the angle of orientation of the prolate spheroid (perpendicular to the major axis Z, see **Fig. 7**) relative to the incident wave. The combined scattering angle-dependent scattering model is then

$$\sigma_{bs}^{res}(ka_{esr},\theta)=\Theta(\theta)\sigma_{bs_0}^{res}(ka_{esr}) \tag{7}$$

For $ka_{esr}\gg 1$, or $ka_{esr}\to\infty$, when the first Fresnel zone is much smaller than the geometry of the target, the backscattering will approach its asymptotic value derived based on the Kirchhoff Approximation (Eq. 64 in Gaunaurd, 1985):

$$\sigma_{bs}^{asymp}(\theta)=\frac{a_1(\theta)a_2(\theta)}{4}, \tag{8}$$

where $a_1(\theta)$ and $a_2(\theta)$ are the radii of curvatures that are orthogonal at the point where the incident wave (angle-dependent) intercepts the surface of the scattering target. For an incident wave impinging on an ellipsoid with an incident angle θ in the X–Z plane, the asymptotic differential backscattering cross-section can be derived as

$$\sigma_{bs}^{asymp}(\theta)=\frac{\sigma_{bs_0}e_{ac}^4}{\left(\sin^2\theta+e_{ac}^2\cos^2\theta\right)^2} \tag{9}$$

where $\theta=0$ is for the broadside incidence:

$$\sigma_{bs_0}=\frac{c^2}{2a}\left(\frac{b^2}{2a}\right)=\frac{c^2}{4}e_{ba}^2, \tag{10}$$

where $e_{ba}=b/a$ and $e_{ba}=1$ for a prolate spheroid. For the case of a sphere, i.e., $a=b=c$, σ_{bs_0} reduces to $a^2/4$, a well-known solution for a perfectly reflecting sphere (Stanton, 1989). To combine Eqs. (7) and (9), for $ka_{esr}\geq k_Ta_{esr}$ we proposed the following transition function (a transient response of a passive electric system to a step function, Alexander and Sadiku, 2013, Ch. 7.5) to form a hybrid scattering model:

$$\begin{aligned}\sigma_{bs}^{hybrid}(ka_{esr},\theta)&=\begin{cases}\sigma_{bs}^{res}(ka_{esr},\theta), & ka_{esr}<k_Ta_{esr}\\ \left[\sigma_{bs}^{asymp}(\theta)-\sigma_{bs}^{res}(k_Ta_{esr},\theta)\right]\\ \quad\times\left(1-e^{-\alpha(ka_{esr}-k_Ta_{esr})}\right)\\ \quad+\sigma_{bs}^{res}(k_Ta_{esr},\theta), & ka_{esr}\geq k_Ta_{esr}\end{cases}\end{aligned} \tag{11}$$

where k_T is the wave number corresponding to the frequency where the transition starts, α is a parameter governing the transition rate (equivalent to the time constant, τ, for a RC circuit).

$$TS^{hybrid}(ka_{esr},\theta)=10\log_{10}\sigma_{bs}^{hybrid}(ka_{esr},\theta). \tag{12}$$

Comparison of this analytical model with the numerical simulations using the Boundary Element Method (BEM) is shown in **Fig. 8**, where we plot the reduced target strength (RTS) as a function of

ka_{esr}.

$$RTS^{hybrid}(ka_{esr},\theta)=10\log_{10}\left(\frac{\sigma_{bs}^{hybrid}(ka_{esr},\theta)}{\sigma_{bs_0}}\right). \quad (13)$$

The transition function, Eq. (11) was chosen quite arbitrary as long as it could produce satisfactory results.

Figure 8 shows the comparison between the reduced target strength (RTS) predicted by using our hybrid model, Eq. (13), and those computed using the boundary element method (BEM) (Katsikadelis, 2016) for backscattering by prolate spheroids with aspect ratios of 1.0 (sphere), 1/2, 1/3, and 1/4. To produce the results shown in **Fig. 8**, the incident angle is set to zero, or normal incidence, and $k_T\ a_{esr}=0.1$. It can be seen that the agreement is very good. An interesting observation is that the ka_{esr} value where the RTS approaches its asymptotic value, decreases with aspect radio, i.e. the more elongated, the fast the scattering to reach its asymptotic value.

To show the angular dependence, we compared the theoretical predictions using Eq. (12) with the measured data published by Foote (1985), as well as the numerical integration based on the Kirchhoff approximation presented with the data (**Fig. 9**). The experimental data were an average of 13 Pollack (*Pollachius pollachius*) and 2 Saithe (*Polllachius virens*) with the root-mean-square (rms) length, height, and width of the swimbladders being 13.0 cm, 1.17 cm, and 1.76 cm, respectively. The

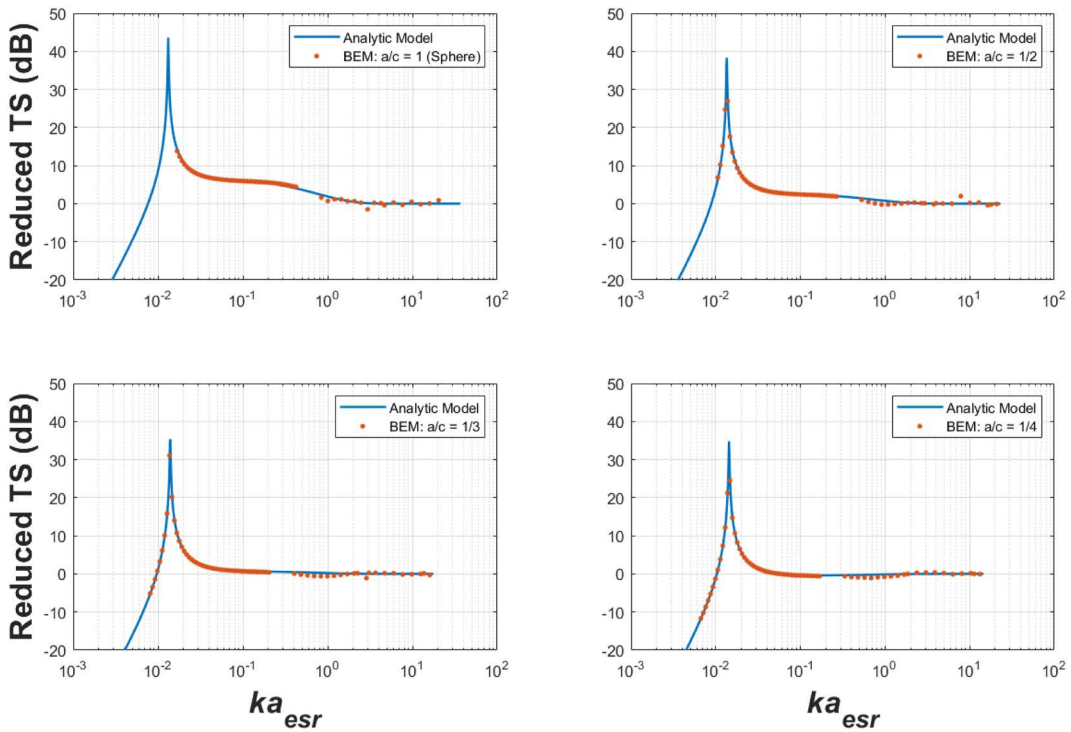

Fig. 8 Comparison of the hybrid scattering model by a prolate spheroidal gas bubble with the numerical simulations using boundary element method (BEM). The four plots correspond to prolate spheroids with aspect radios of 1.0 (sphere), 1/2, 1/3, and 1/4, respectively. In each of the plots, the horizontal axis is the dimensionless parameter, ka_{esr}, where k is the acoustic wavenumber, and a_{esr} is the equivalent spherical radius (equal volume). The vertical axis is the reduced target strength (RTS) defined in Eq. (13) and $k_T a_{esr}=0.1$.

Kirchhoff model used by Foote (1985) was frequency dependent model, and the integration was done numerically involving a series of digitized cross sections of swimbladders cut with a microtome and photographed at intervals varying from 200 to 1400 μm (Foote, 1985). The theoretical model predictions of the fish target strength (TS) were calculated using Eq. (12) with the following computation parameters for a prolate spheroid: semi-major axis $c=13/2=6.5$ cm, semi-minor axis $a=\sqrt{(1.17\times1.76)}/2=0.72$ cm (equivalent area of a circle), and the $ka_{esr}=3.6$ at 120 kHz, which is in the geometric scattering region and basically approaches the asymptotic scattering level (**Fig. 8**). It can be found that the hybrid scattering model provided much more smoothed curves than the Kirchhoff Approximation integral since the former uses a much simpler geometry to approximate the real shape of swimbladders of 15 individual fish.

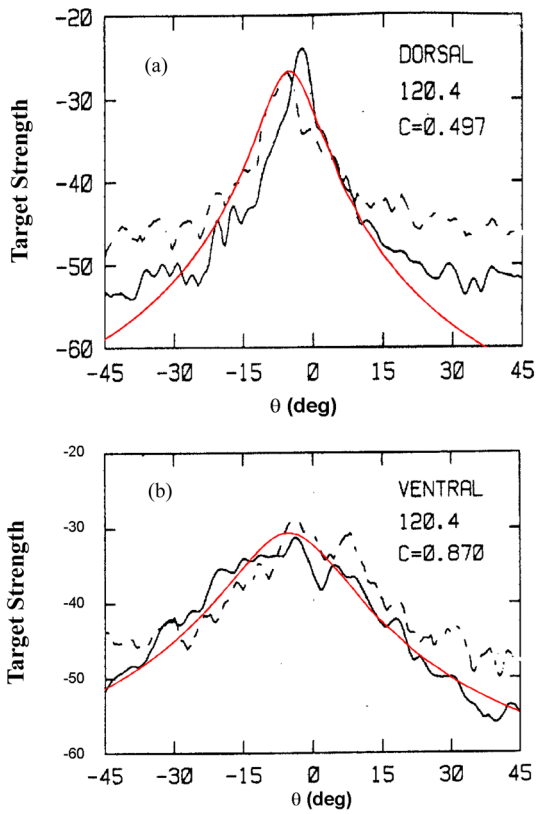

Fig. 9 Comparison of the experiment data (dashed line) and Kirchhoff model (solid black line) (adapted from Foote, 1985, with permission) and those computed using Eq. (12) (solid red line). The TS of the experiment data were an average of 13 *Pollachius pollachius* and 2 *Polllachius virens* with the rms length, height, and width of the swimbladders being 13.0 cm, 1.17 cm, and 1.76 cm, respectively. The Kirchhoff model used by Foote (1985) was frequency dependent model, and the integration was done numerically (solid black line). The theoretical TS predictions of the hybrid scattering model using Eq. (12) used the following computation parameters for a prolate spheroid: semi-major axis $c=13/2=6.5$ cm, semi-minor axis $a=\sqrt{(1.17\times1.76)}/2=0.72$ cm (equal area of a circle).

2.3.2 Scattering by fish without swimbladders

For fish without swimbladders, the whole fish can be approximated as a weakly scattering target with homogeneous material properties inside fish body. The backscattering of a weakly scattering object of an arbitrary shape can be approximated by an integral form of a volume (v_0) based on the Distorted Wave Born Approximation (DWBA) (Chu *et al*., 1993; Stanton *et al*., 1998b):

$$f_{scat}^{DWBA}=\frac{k_1^2}{4\pi}\int_{v_0}\left(h^2\gamma_k+\hat{\mathbf{k}}_\mathbf{i}\cdot\hat{\mathbf{k}}_\mathbf{s}\gamma_\rho\right)e^{ik_2\left(\hat{\mathbf{k}}_\mathbf{i}-\hat{\mathbf{k}}_\mathbf{s}\right)\cdot r_0}dv_0 \quad (14)$$

where $k_{1,2}$ are the wave numbers in media 1 (surrounding water) and 2 (scatterer), respectively. r_0 is the position vector inside the scatterer, and $\hat{\mathbf{k}}_\mathbf{i}$ and $\hat{\mathbf{k}}_\mathbf{s}$ are unit vectors of the incident and scattered wavenumbers, respectively. $h=k_1/k_2=c_2/c_1$ is the sound speed contrast of the animal. By using a density contrast $g=\rho_2/\rho_1$, we can express γ_k and γ_ρ as

$$\gamma_\kappa=\frac{1-gh^2}{gh^2} \quad \text{and} \quad \gamma_\kappa=\frac{g-1}{g} \quad (15)$$

With the geometry shown in **Fig. 7**, the two unit-vectors are

$$\hat{\mathbf{k}}_\mathbf{i}=\cos\theta_i\cos\phi_i\,\hat{x}+\cos\theta_i\sin\phi_i\,\hat{y}+\sin\theta_i\,\hat{z} \quad (16)$$

$$\hat{\mathbf{k}}_\mathbf{s}=\cos\theta_s\cos\phi_s\,\hat{x}+\cos\theta_s\sin\phi_s\,\hat{y}+\sin\theta_s\,\hat{z} \quad (17)$$

where (θ, ϕ) are spherical angles (polar and azi-

muth) in the spherical coordinates. In deriving Eq. (14), the unknown wave number $\vec{\mathbf{k}}_s$ of the integrand in the exact Helmholtz-Kirchhoff integral equation (Morse and Ingard, 1968) is replaced with the local wave number inside the scattering body, $\vec{\mathbf{k}}_\mathbf{s}=k_s\hat{\mathbf{k}}_\mathbf{s}\approx k_2\hat{\mathbf{k}}_\mathbf{s}$, (Chu *et al*., 1993).

There are many publications of applying the DWBA to weak scattering objects, such as zooplanktons with complicated shapes (Stanton *et al*., 1998a; Chu and Ye, 1999; Lavery *et al*., 2002; Chu *et al*., 2016). A link providing more potential applications of the DWBA with various geometric shapes and material properties is given by Gastauer *et al*. (2019).

To study the scattering by fish body (no swimbladder), we can use an ellipsoid to approximate the geometric shape of a fish body. To simplify the derivation, we assume that the material properties of the fish are homogeneously distributed inside the body, i.e. γ_k and γ_ρ defined in Eq. (15) are constants inside the entire integration volume. It is straightforward to show that the scattering amplitude of an ellipsoid can be expressed as a compact and analytical form (Chu *et al*., 2008):

$$f_{scat}^{DWBA} = k_1^2\left(h^2\gamma_k-\gamma_\rho\right)abc\frac{j_1\left(k_2a\sqrt{\Pi_\mathrm{x}^2+e_{ba}^2\Pi_\mathrm{y}^2+e_{ca}^2\Pi_z^2}\right)}{k_2a\sqrt{\Pi_\mathrm{x}^2+e_{ba}^2\Pi_\mathrm{y}^2+e_{ca}^2\Pi_z^2}} \tag{18}$$

where $j_1(x)$ is the spherical Bessel function of order 1, and $e_{ba}=b/a$, $e_{ca}=e_{ac}^{-1}=c/a$.

$$\begin{aligned}\Pi_\mathrm{x}&=\cos\theta_i\cos\phi_i-\cos\theta_s\cos\phi_s\\ \Pi_\mathrm{y}&=\cos\theta_i\sin\phi_i-\cos\theta_s\sin\phi_s\\ \Pi_z&=\sin\theta_i-\sin\theta_s\end{aligned} \tag{19}$$

For a backscattering scenario, which is the case for most applications in fisheries acoustics, $\hat{\mathbf{k}}_\mathbf{i}\cdot\hat{\mathbf{k}}_\mathbf{s}=-1$, $\theta_i=\pi-\theta_s$ and $\phi_i=\pi+\phi_s$, the three sine and cosine items in Eq. (19) are

$$\begin{aligned}\Pi_\mathrm{x}&=-2\cos\theta_s\cos\phi_s\\ \Pi_\mathrm{y}&=-2\cos\theta_s\sin\phi_s\\ \Pi_z&=-2\sin\theta_s\end{aligned} \tag{20}$$

Note that $\theta_s=0$ corresponds to the broadside incidence with $\phi_s=0$, for incident wave along x-axis (X–Z plane) while $\phi_s=\pi/2$ for incident wave along y-axis (Y–Z plane).

3. Application examples

In this section, we present a few examples to show (1) applications of broadband technology to characterize the acoustic scattering by different targets, and (2) an application of conducting an acoustic survey using USVs.

3.1 Broadband systems

3.1.1 Spectral characterization of fish and zooplankton

A field application of a towed broadband system, EdgeTech as described earlier in Section 2.1.5, was carried out during a herring survey aboard the NOAA Ship Fisheries Research Vessel (FRV) *Delaware II* over Georges Bank off Cape Cod, MA in the period 7–15 September 2005 (Stanton *et al*., 2010). The FRV *Delaware II* was equipped with the standard Simrad EK500 narrow-band echosounders, with the calibration conducted in the field during the cruise. The calibration of the towed EdgeTech calibration was conducted post-cruise off Provincetown, Cape Cod, MA using a small R/V *Tioga*. A comparison of the 120 kHz narrow-band echosounder and the broadband echosounder of EdgeTech (6–17 kHz) is illustrated in **Fig. 10**. The pulse duration of the narrow-band echosounder was 1.024 ms, while the bandwidth of

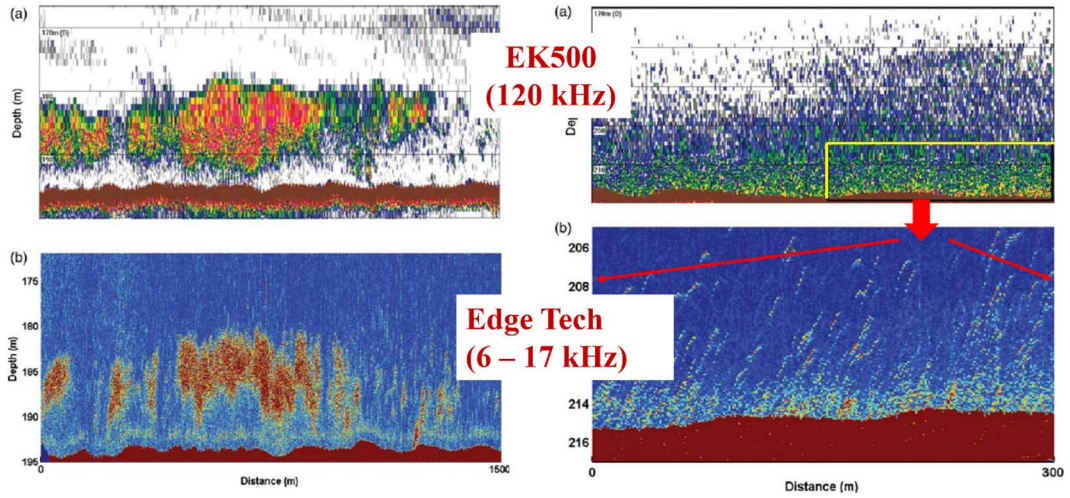

Fig. 10 Comparison of the echograms recorded with Simrad EK500 120 kHz narrow-band echosounder (adapted from Stanton *et al*., 2010, with permission). The pulse duration of the narrow-band echosounder was 1.024 ms, while the bandwidth of the EdgeTech broadband echosounder (channel 424, see Table 2) was about 10 kHz (6–17 kHz). The EdgeTech echograms were displayed after pulse-compressing process (Chu and Stanton, 1998). The two echograms on top panels are from the narrow-band data while the bottom two panels are from broadband data.

the EdgeTech broadband echosounder was about 10 kHz (6–17 kHz). The EdgeTech echograms were displayed after pulse-compressing process (Chu and Staton, 1998), which provided much higher range resolution.

The spectral characterization of the volume backscattering strength, $S_v = 10\log_{10} s_v = 10\log_{10}(n\sigma_{bs})$, from different marine organisms shown in **Fig. 11** (adapted from Stanton *et al*., 2010), where σ_{bs} represents the average differential backscattering cross section of an individual target, and n is the number density of the scattering targets within the acoustically insonified volume. Backscattering by herring, depicted in **Fig. 11**(a), clearly demonstrates the resonance phenomenon observed in two separate patches or aggregations. The dense patch corresponds to the large central aggregation in **Fig. 10** (lower-left plot), and the sparse patch corresponds to one of the small patches nearby. The three segments of data correspond to the three broadband acoustic channels, i.e., Shamu (low frequency), 424 (mid-frequency), and Reson (high frequency)—each detailed in **Table 2**. A significant advantage of the EdgeTech system is its low frequency channel (Shamu) that encompasses the resonance frequency of many fish species, such as herring in this application. The fact that the resonance patterns (frequency responses) being consistent for both patches suggest they comprised herrings of the same size; the mean strength of the patches reflected the numerical density of the fish aggregations, estimated at 0.3 and 0.05 m^{-3} for the denser and sparser patches, respectively. The two thick solid black curves represent the theoretical model predictions, combing the resonance scattering model (Love, 1978) with the deformed cylinder model (Stanton, 1989).

The backscattering from a near-surface daylight swarm [**Fig. 11**(b)] appeared to originate from weak scattering zooplankton in mostly the Rayleigh scattering region, transitioning to the geometric scattering around 85 kHz—consistent with elongated fluid-like scatterers approximately 5 cm long. The spectral data were recorded with

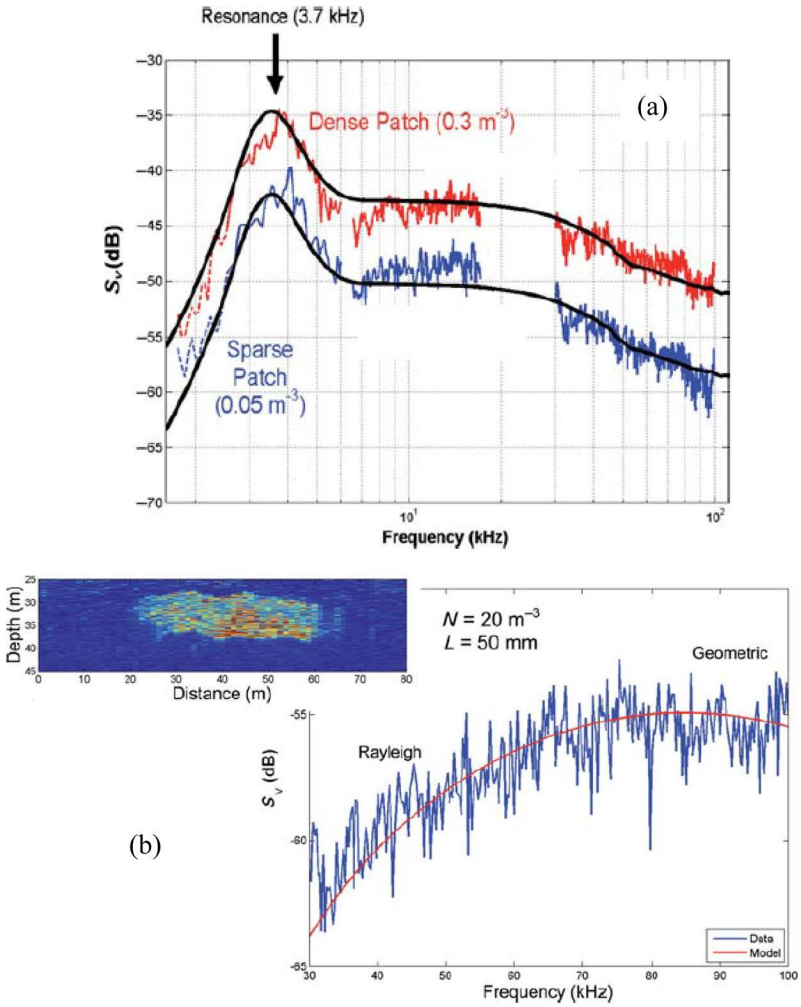

Fig. 11 Spectral characterization of volume backscattering strength, S_v, from different marine organisms (adapted from Stanton *et al*., 2010, with permission). (a) Resonance phenomenon observed in two separate patches of herring. The three segments of data correspond to the three broadband acoustic channels (Shamu, 424, and Reson, Table 2). The thick solid lines are predictions from the theoretical scattering model and the numbers are estimated numerical density of herring. (b) S_v of a near-surface daylight swarm of what appears to be zooplankton (~50 mm long). Estimated numerical density is N=20 m^{-3}. The transition from Rayleigh to geometric scattering is at about 85 kHz. The red solid line is the model prediction based on the DWBA.

the high frequency channel (Reson). We fitted the DWBA model of an elongated cylinder (Staton *et al*., 1998b) to the measured data and obtained a numerical density estimation of about 20 animals per m^3 (Staton *et al*., 2010). Although the aggregations were not directly sampled during the time of data recording, their form and timing were consistent with swarming behavior when they were attacked by predators (Nøttestad, 1988).

3.1.2 Nearfield calibration using a standard target

Calibrating broadband echosounder systems accurately and reliably in the farfield can be challenging due to the extended distance required for farfield conditions. For instance, with the Simrad ME70 multi-beam system operating at 120 kHz, the farfield distance, calculated using the formula

$r_F=D^2/\lambda$, where D is the diameter of the transducer and λ is the wave length of the transmitted pulse, turns out to be approximately 20 meters. This distance complicates the calibration setup and maneuverability significantly.

To address the farfield calibration difficulties, a method of conducting a nearfield calibration and extending the resultant parameters to farfield applications, was developed by Chu and Eastland (2015). This method was implemented during a calibration experiment at the NOAA Fisheries Northwest Fisheries Science Center (NWFSC) in 2013. The experiment setups, as illustrated in **Fig. 12**, utilized a pair of custom-made broadband transducers made of 1–3 composite materials (Material System, Inc., Littleton, MA). These transducers had a maximum amplitude between 550 and 600 kHz and a nominal bandwidth of about 200 kHz. The experiment configuration was a pseudo-monostatic, with two transducers adjacent to each other to simulate a backscattering scenario.

A 25-mm tungsten carbide sphere (WC25) was used and placed at 8.25, 9.25, 10.25, 11.25, and 15.25 cm away from the center of the two transducers. Based on the formula $r_F=D^2/\lambda$, the estimated farfield distances were about 8.3 cm at 200 kHz, and 37.5 cm at 900 kHz. **Figure 13**(a) illustrates the measured frequency responses of the received pulses at 8.25, 11.25, and 15.25 cm, demonstrating that at low-frequency end, all curves are closely aligned, whereas at the high-frequency end, the spectrum corresponding to 8.25 cm shows a greater decrease more than that at 15.25 cm, highlighting the influence of nearfield effects. The theoretical predictions of the frequency responses at the farfield and the near field at those three distances are displayed in **Fig. 13**(b), where the transducer frequency response was excluded.

The theoretical predictions of the bi-scattering by a calibration (elastic) sphere can be expressed as a quadruple integration over the transmit and receive transducer surfaces as (Chu and Eastland, 2015)

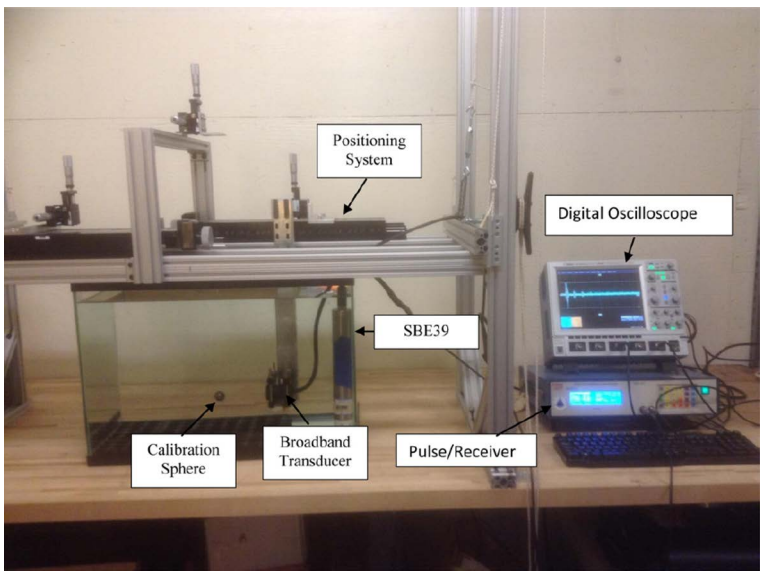

Fig. 12 Photograph depicting the setup of the laboratory experiment system used for nearfield calibration, as originally shown in Chu and Eastland (2015, with permission).

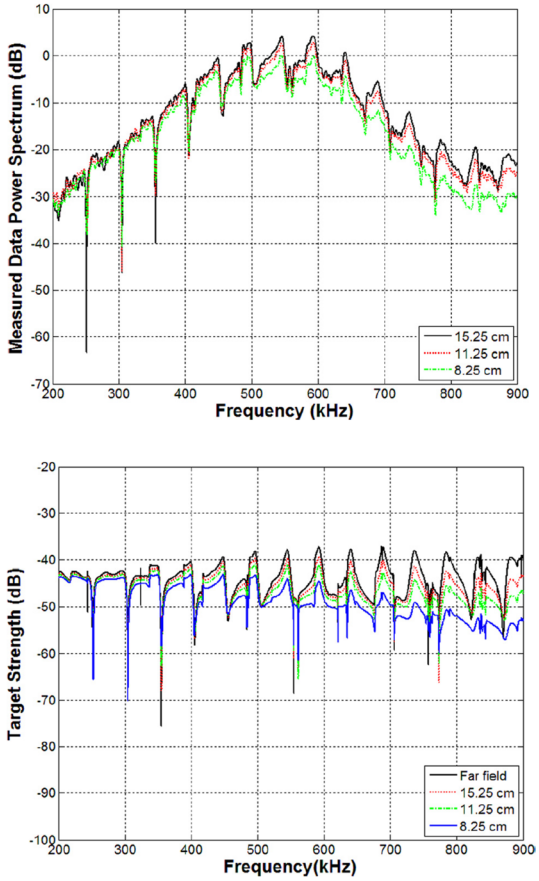

Fig. 13 Measured and modeled nearfield responses of a 25-mm tungsten carbide sphere. (a) Measured spectra derived from the recorded data at ranges at 8.25, 11.25, and 15.25, respectively. (b) Theoretical predictions of the corresponding near-field spectra at the 5 ranges given in (a), and the farfield spectrum (directly taken from Chu and Eastland, 2015, with permission).

$$p_{scat}(\vec{\mathbf{r}}_{\mathbf{R}};\vec{\mathbf{r}}_{\mathbf{T}}) = \frac{1}{A_T A_R}\iint_{A_T}\iint_{A_R} p_s(\vec{\mathbf{r}}_{\mathbf{r}};\vec{\mathbf{r}}_{\mathbf{s}})\,dA_T dA_R$$
$$= \frac{ip_0 kr_{ref}}{A^2}\iint_{A_T}\iint_{A_R}\sum_{n=}^{\infty} \times c_n(2n+1)h_n^{(2)}(kr_r)h_n^{(1)}(kr_s) \times P_n(\cos\theta)\,dA_T dA_R \tag{21}$$

where p_s ($\vec{\mathbf{r}}_{\mathbf{r}}$; $\vec{\mathbf{r}}_{\mathbf{s}}$) is the pressure of the bistatic scattering by a target (WC25) with a point source and a point receiver; $\vec{\mathbf{r}}_{\mathbf{T}}$ and $\vec{\mathbf{r}}_{\mathbf{R}}$ are vectors from the center of the scatterer to the center of the transmitter and receiver, respectively; $\vec{\mathbf{r}}_{\mathbf{s}}$ and $\vec{\mathbf{r}}_{\mathbf{r}}$ are the vectors from the center of the scatterer to an arbitrary point on the surfaces of the transmitter and receiver, respectively. The two double integrals are over the transducer surfaces of the transmitter (A_T) and receiver (A_R), respectively. $h_n^{(1)}(x)$ and $h_n^{(2)}(x)$ are the spherical Hankel functions of the first and second kind. $P_n(x)$ is the Legendre polynomial of degree n, and the angle is the angle between the two position vectors, $\vec{\mathbf{r}}_{\mathbf{s}}$ and $\vec{\mathbf{r}}_{\mathbf{r}}$. The coefficient c_n is given explicitly by Faran (1951). p_0 is the pressure at a reference range, r_{ref}. In addition, the fact that the two transducers were identical leads to A_T=A_R=A. More details regarding the experiment setups and system configuration, and the data processing can be found in Chu and Eastland (2015).

A calibration curve as a function of frequency was obtained by smoothing out the points around nulls as detailed in Chu and eastland (2015). The comparisons of the measured data with the predicted TS after applying the calibration curve at different depths are displayed in **Fig. 14**. The figure demonstrated that there is a reasonable agreement between model predictions and the experiment data over a wide frequency band, ranging from 300 to 900 kHz, which is three times wider than the nominal bandwidth. The overall root-mean-square (rms) mismatch was about 1.0 dB when nulls were included and reduced to less than 0.5 dB (0.34 ± 0.02 dB) when nulls were excluded (**Table 4**). This demonstrates the effectiveness of the calibration method in addressing the complexities associated with farfield calibration in broadband echosounder systems.

The findings from this approach are highly promising for applying the calibration conducted with nearfield configuration to the farfield applications. This method potentially simplifies the calibration

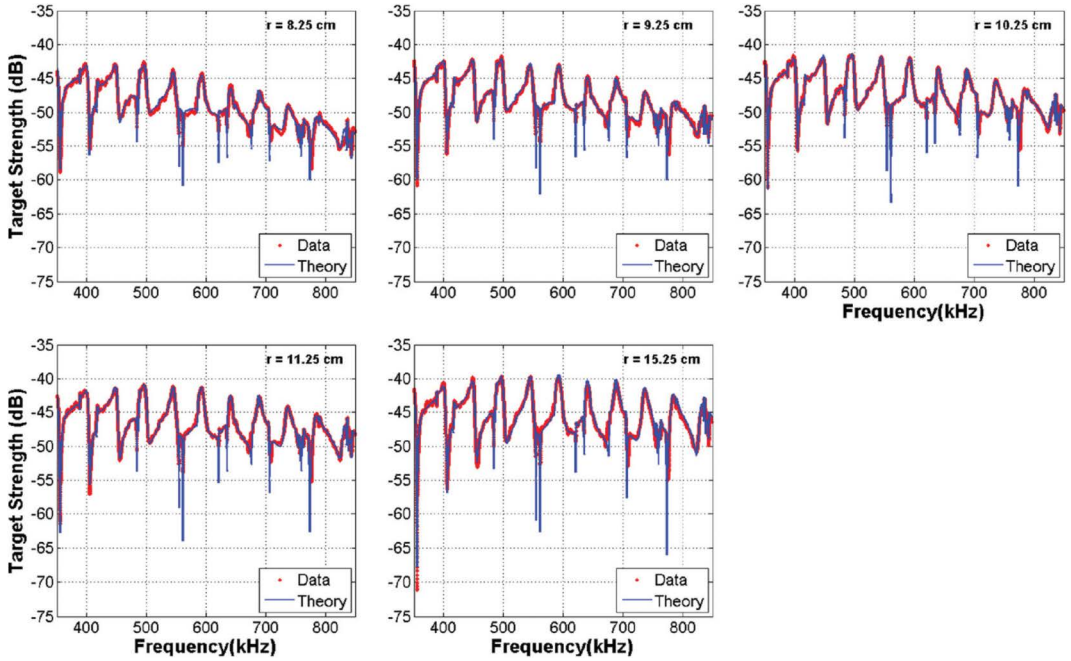

Fig. 14 Comparison of the measured nearfield data with the corresponding theoretical model predictions for data recorded when the sphere was at ranges of 8.25, 9.25, 10.25, 11.25, and 15.25, respectively (directly taken from Chu and Eastland, 2015, with permission).

Table 4 Comparison of the model predictions and the measured near-field spectra. The frequency range is from 300 to 900 kHz as shown in Fig. 14.

Range (cm)	8.25	9.25	10.25	11.25	15.25	Mean ± s.d
rms calibration uncertainty (dB) (nulls included)	0.90	0.91	1.01	1.00	1.32	1.03 ± 0.17
rms calibration uncertainty (dB) (nulls excluded)	0.34	0.31	0.34	0.34	0.37	0.34 ± 0.02

process, particularly in terms of the calibration gear and setups required, which is especially beneficial for future application of multi-beam systems (Gerlotto *et al*., 1994; Foote *et al*., 2005; Trenkel *et al*., 2008; Ona *et al*., 2009; Misund and Coetzee, 2000). This simplification could lead to more efficient and accessible calibration protocols for complex multi-beam echosounder systems, ultimately enhancing the accuracy and reliability of acoustic measurements in marine research.

3.2 Sampling platforms

The integration of autonomous vehicles into ocean sciences has shown significant promise, (Widditsch, 1973; Kosalos and Chayes 1983; Jarry, 1986; Tyce, 1986; Jaffe *et al*., 2001; Greene *et al*., 2014; Wynn *et al*., 2014; Moline *et al*., 2015). However, using autonomous vehicles to conduct fisheries acoustic surveys had not been reported until late 2010's (DeRobertis *et al*., 2019, 2021; Chu *et al*., 2019, 2021). These studies primarily utilized Saildrones (https://www.saildrone.com/), a type of Uncrewed Surface Vehicles (USVs), renowned for their long endurance, data quality, and operational convenience (**Table 3**).

De Robertis and his colleagues (2019) conducted a comprehensive survey of walleye pollock (*Gadus chalcogrammus*) for 103 days in Bering

Sea, involving both NOAA Ship Fisheries Survey Vehicle (FSV) *Oscar Dyson* and three Saildrones (De Robertis *et al*., 2019). Opportunistic comparisons indicated that backscatter paths were similar where the FSV and USVs crossed. Overall, for the acoustic data collected with Simrad EK80 38-kHz echosounders, Saildrone (SD) detected equivalent backscatter to within 10% of that of FSV.

Here we present another survey example to compare the acoustic backscatter recorded with the echosounders mounted on FSV and USVs (Chu *et al*., 2021) based on a coast-wide survey. A Biennial Pacific Hake (*Merluccius productus*) acoustic survey was conducted from June 15 to August 21, 2019 (68 days) for FSV Bell Shimada and from June 17 to August 25 (70 days) for SDs. There were total of five SDs operated during the survey, ensuring four SDs working at sea at the same time to collect acoustic survey data. The coast-wide Pacific hake survey was conducted from south to north spanned a distance of about 850 nautical miles (nmi), or more than 1,500 km. Both FSV and SDs were running the same transects. A total of 85 transects were surveys and 68% of time the FSV and SDs were overlapped within ±3 days, and 84% within ±5 days. Two SDs were switched due to technical malfunction, which was repaired in-field quickly. The total distance that the SDs surveyed was 2,845 nmi, or about 5,270 km with an average survey speed of 2.1 knots, about 1/5 of the FSV survey speed (10 knots).

The 2D map of the acoustic backscatter comparison is shown in **Fig. 15**, where the red circles represent the nautical areal scattering coefficient (NASC or s_A), and the diameter of the circle reflects the value of NASC indicated in the figure legend. Observation of these two maps reveals that the overall distribution is similar but there are many differences. For example, there are places where noticeable backscatters (red circles) can be seen in the FSV's NASC map between transect 70 and 80 (left) while only very few backscatters (red circles) on the SD's NASC map (right). In contrast, on transects 5 and 6 in the south, red circles can be clearly identified on SD's NASC map, while there are basically no red circles on the FSV's NASC map. These differences may due to the time difference when the FSV and SDs surveyed the transects, reflecting dynamic feature of hake distribution. Over all depth distribution comparison is shown in **Fig. 16**, while the left plot is the average NASC vertical profile, the right plot is the cumulative NASC distribution. Although the absolute NASC values are different, their relative or normalized cumulative NASC profiles are very similar.

In fisheries science, understanding the distribution of biomass or abundance at age is crucial for effective stock assessment. The comparison of estimated biomass at age distributions based on the acoustic data collected with FSV and SDs is illustrated in **Fig. 17**. There are some differences between the two histograms, SD's histogram over-estimates ages 3, 7, and 9 while the FSV's histogram over-estimates ages 2, 3, and 8. However, over all distribution pattern agrees with each other reasonably well. The comparison of the total biomass and the corresponding coefficient of variance (CV) are provided in **Table 5**. The total biomass estimated based on the SD data was about 21% less than that of FSV's. The CVs that were estimated with Kriging (Deutsch and Journel, 1992; Journel and Huijbregts, 1992; Kitanidis, 1997) and Jolly-Hampton's method (Jolly and Hampton, 1990) based on the SD data were all larger than those of FSV's.

There are a few possible explanations for these differences. One of the most important is that there were many biological samplings (trawls) at about

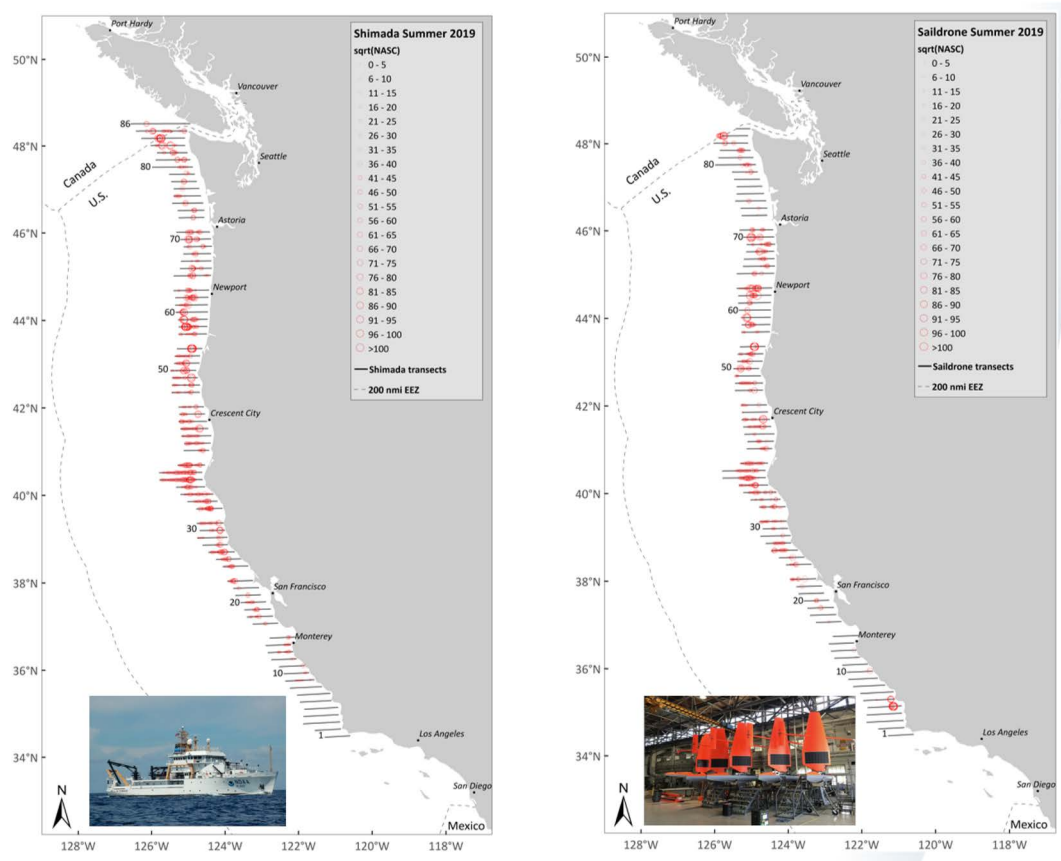

Fig. 15 Comparison of the 2-D NASC maps based on acoustic data collected with centerboard-mounted echosounders with that obtained from USV-mounted echosounders (Chu *et al*., 2021).

the same time as the acoustic data were collected to verify the hake identification/classification during the FSV survey while identification/classification of hake aggregations using the SD's data was purely based on the knowledge and experience of the scientists who processed and interpreted the acoustic raw data. Second, FSV had five frequencies while the SD was only equipped two frequencies, which made the scientists much hard and less confident in identifying the hake aggregations. Third, due to the dynamic features of Pacific hake, difference in time acoustic data recording would also likely lead to the discrepancy in acoustic backscatter.

Despite these differences, the application of SDs to fisheries acoustic surveys offers significant advantages including (1) flexibility in survey time and area; (2) more cost effective; (3) more resilient to harsh weather; (4) more environment friendly.

It can be envisioned that while the fisheries acoustic surveys using AUVs including USVs are unlikely to replace the ship-based surveys, they are poised to significantly enhance the capability, efficiency, and flexibility of traditional ship-based fisheries acoustic surveys. The integration of USVs into fisheries research and surveys represents a forward-looking approach to oceanographic studies, promising to expand the scope and scale of monitoring and conservation efforts significantly.

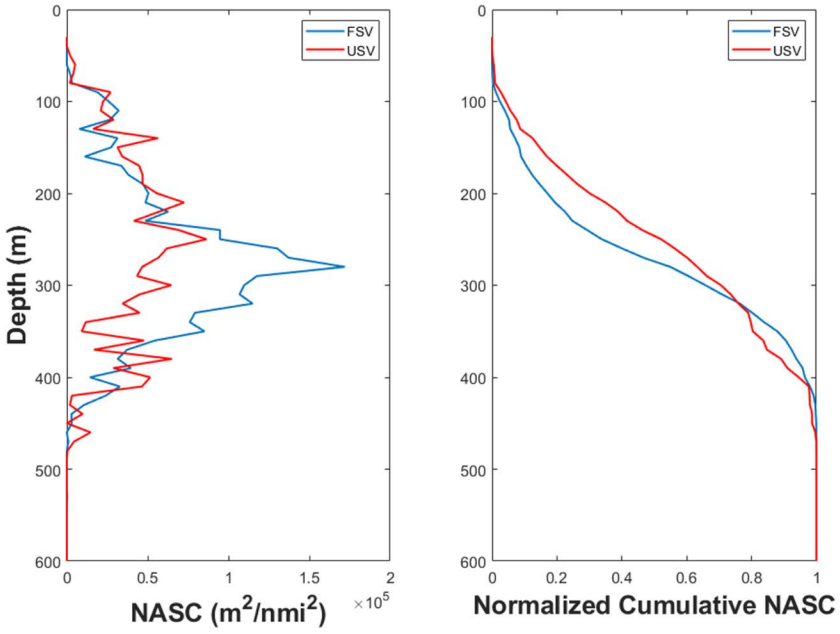

Fig. 16 Comparison of the 1-D NASC profiles based on acoustic data collected with centerboard-mounted echosounders with those obtained from USV-mounted echosounders (directly taken from Chu *et al*., 2021).

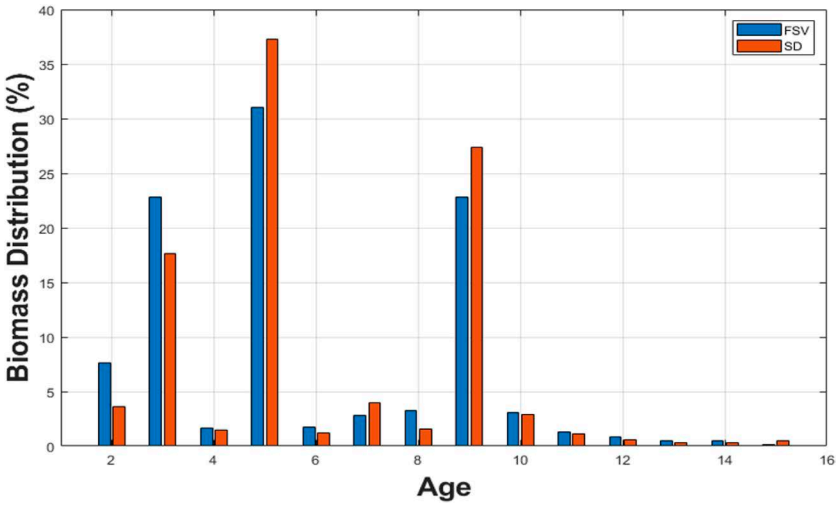

Fig. 17 Comparison of the histogram of biomass at age based on acoustic data collected with centerboard-mounted echosounders with that obtained from USV-mounted echosounders (directly taken from Chu *et al*., 2021).

Table 5 Comparison of Pacific hake biomass estimates (million-metric-tons, mmt) between those estimated with FSV and USV acoustic data, where CV (Krig) is estimated CV based on the Kriging and CV (J–H) is the estimated CV based on the method proposed by Jolly and Hampton (1990).

Biomass-FSV			Biomass-USV			Biomass Difference (%)
US (mmt)	CV (krig)	CV (J–H)	US (mmt)	CV (krig)	CV (J–H)	
1.485	6.33%	13.95%	1.168	9.71%	16.38%	− 21.4%

4. Summary

Acoustic technologies have been a cornerstone in fisheries science for nearly a century, evolving significantly over this period. Initially, these technologies were basic, consisting of single-frequency, single-beam systems that provided only qualitative data. Today, they have transformed into sophisticated multi-frequency, multi-beam systems that are calibrated and quantitative. This paper explores the science and technology advancements in this field, covering developments in echosounder hardware, data acquisition platforms, and theoretical acoustic scattering models. The theoretical acoustic scattering models initially focused on simple models such as spherical bubbles and evolved to current more complicated shapes, enhancing the accuracy and utility of acoustic data in fisheries research.

Acknowledgement

The author expresses his profound gratitude to his esteemed colleagues in Japan for their generous hospitality and the meticulous organization of his visit, including Drs. Kouichi Sawada, Ryodo Kawasaki, Tohru Mukai, Kazuo Amakasu, and Yoshiaki Fukuda. The research work discussed in this paper received partial funding from the US Office of Naval Research, the Woods Hole Oceanographic Institution (WHOI), the US NOAA Fisheries, and the Northwest Fisheries Science Center (NWFSC). Special thanks are extended to colleagues at WHOI and NWFSC for their invaluable support and assistance with the research presented herein. Additionally, a heartfelt thank you to Dr. Sven Gastauer for providing the Boundary Element Method (BEM) numerical computations of backscattering by a prolate spheroidal gas, which significantly contributed to this study.

References

Alexander, C. K., and Sadiku, M. N. O., 2013. *Fundamentals of electric circuits*. 5th ed., McGraw-Hill, New York.

Ainslie, M. A. and Leighton, T. G., 2011. Review of scattering and extinction cross-sections, damping factors and resonance frequencies of a spherical gas bubble. J. Acoust. Soc. Am., **130**: 3184: 3208. DOI: 10.1121/1.3628321.

Anderson, V. C., 1950. Sound scattering from a fluid sphere. J. Acoust. Soc. Am., **22**: 426–431. https://doi.org/10.1121/1.1906621.

Andreeva, I. B., 1964. Scattering of sound by air bladders of fish in deep sound-scattering ocean layers. Sov. Phys. Acoust., **10**: 17–20.

Anon, 1934. Forsokene med ckkolodd ved Brislingfisket (Trail with an echosounder during the sprat fishery). Tiddsskrift for Hermetikindustri (Bulletin of the Canning Industry), July, pp. 222–223. (in Norwegian).

Anon, 1965. Report of the third meeting of the Atlantic-Scandian herring working group. ICES, C.M. 1965/161 (Mimeo).

Anon, 1967. Preliminary report of the international 0-group fish survey in the Barents Sea and adjacent waters August/September 1967. ICES, C.M. 1967/H:31

Anson, L., and Chivers, R., 1993. Ultrasonic scattering from spherical shells including viscous and thermal effects. J. Acoust. Soc. Am., **93**: 1687–1699.

Benoit-Bird, K. J., Welch, T. P., Waluk, C. M., Barth, J. A., Wangen, I., McGill, P., Okuda, C. *et al.* 2018. Equipping an underwater glider with a new echosounder to explore ocean ecosystems. Limnol. Oceanogr.: Methods, **16**: 734–749.

Brede, B., 1984. SIMRAD EK-400 scientific echo

sounder. FAO Fish. Circ., **778**: 44–56.

Brehmer, P., Gerlotto, F., and Samb, B., 2000. Measuring fish school avoidance during acoustic surveys. Incorporation of external factors in marine resources survey. ICES CM 2000/K:07.

Chu, D., Foote, K. G., Stanton, T. K., 1993. Further analysis of target strength measurements of Antarctic krill at 38 kHz and 120 kHz: Comparison with deformed cylinder model and inference of orientation distribution. J. Acoust. Soc. Am., **93**: 2985–2988.

Chu, D. and Stanton, T. K., 1998. Application of pulse compression techniques to broadband acoustic scattering by live individual zooplankton. J. Acoust. Soc. Am., **104**: 39–55.

Chu, D. and Ye, Z., 1999. A phase-compensated distorted wave Born approximation representation of the bistatic scattering by weakly scattering objects: Application to zooplankton. J. Acoust. Soc. Am., **106**: 1732–1743.

Chu, D., 2011. Technology evolution and advances in fisheries acoustics. J. Mar. Sci. Tech., **19**: 245–252.

Chu, D., Stanton, T. K., and Jech, J. M., 2008. Modeling of broadband backscattering by swimbladder-bearing fish over a wide range of frequencies. Presentation at the International Council for the Exploration of the Sea (ICES), the 2008 Symposium on the Ecosystem Approach with Fisheries Acoustics and Complementary Technologies (SEAFACTS), 16–20 June 2008, Bergen, Norway.

Chu, D. and Eastland, G. C., 2015. Calibration of a broadband acoustic transducer with a standard spherical target in the near field. J. Acoust. Soc. Am., **137**: 2148–2157.

Chu, D., Lawson, G. L., and Wiebe, P. H., 2016. Estimation of size, orientation, and abundance of marine organisms using acoustic scattering model-based inversions. J. Acoust. Soc. Am., **139**: 2885–2895. http://dx.doi.org/10.1121/1.4948759

Chu, D., Parker-Stetter, S., Hufnagle, L. C., Gauthier, S., Thomas, R., Stanley, C., and Getsiv-Clemons, J., 2019. 2018 Unmanned Surface Vehicle (Saildrone) acoustic survey off the west coasts of the United States and Canada. Proceedings of the MTS/IEEE Oceans 2019, Seattle, WA. doi: 10.23919/OCEANS40490.2019.8962778

Chu, D., Clemons, J., de Blois, S., Gauthier, S., Hufnagle, L. C., Parker-Stetter, S., Pohl, J., Stanley, C., and Thomas, R., 2021. Comparison of abundance and biomass estimates from an acoustic survey conducted by a NOAA Fisheries Survey Vessel and Uncrewed Surface Vehicles. Presentation at the 2021 Annual meeting of the Working Groug of the Fisheries Acoustics Science and Technology (WGFAST) of International Council for the Exploration of the Sea (ICES) (online virtual meeting).

Cochrane, N. A., Li, Y. and Melvin, G. D., 2003. Quantification of a multibeam sonar for fisheries assessment applications. J. Acoust. Soc. Am., **114**: 745–758.

Cushing, D. H., 1952. Echo-survey of fish. Journal du Conseil Permanent International pour l'Exploration de la Mer, **18**: 45–60.

Cutter, G. R. Jr., Stierhoff, K. L. and Demer, D. A., 2016. Remote sensing of habitat characteristics using echo metrics and image-based seabed classes. J. Mar. Sci., **73**(8): 1965–1974. doi: 10.1093/icesjms/fsw024.

Dalen, J., Nedreaas, K., and Pedersen, R., 2003. A comparative acoustic-abundance estimation of pelagic redfish (*Sebastes mentella*) from hull-mounted and deep-towed acoustic systems. ICES J. Mar. Sci., **60**: 472–479.

Demer, D. A., Berger, L., Bernasconi, M., Bethke,

E., Boswell, K., Chu, D., Domokos, R., *et al.*, 2015. Calibration of acoustic instruments. ICES Cooperative Research Report No. 326. p. 133.

De Robertis, A., Lawrence-Slavas, N., Jenkins, R., Wangen, I., Mordy, C. W., Meinig, C., Levine, M., Peacock, D. and Tabisola, H., 2019. Long-term measurements of fish backscatter from Saildrone unmanned surface vehicles and comparison with observations from a noise-reduced research vessel. ICES J. Mar. Sci., **77**(2): 765–775. DOI: 10.1093/icesjms/fsaa005

De Robertis, A., Levine, M., Lauffenburger, N., Honkalehto, T., Ianelli, J., Monnahan, C., C., Towler, R., Jones, D., Stienessen, S. and McKelvey, D., 2021. Uncrewed surface vehicle (USV) survey of walleye pollock, *Gadus chalcogrammus*, in response to the cancellation of ship-based surveys. ICES J. Mar. Sci., **78**: 2797–2808.

Deutsch, C. V. and Journel, A. G., 1992. *GSLIB: Geostatistical Software Library and User's Guide*. Oxford University Press, Oxford, p. 340.

Dragesund, O. and Olsen, S., 1965. On the possibility of estimating year-class strength by measuring echo-abundance of 0-group fish. Fiskeri Dir. Slrr. Ser. Havunders, **13**(8): 48–75.

Dragonette, L. R., Numrich, S. K., and Frank, L. J., 1981. Calibration technique for acoustic scattering measurements. J. Acoust. Soc. Am., **69**: 1186–1189.

Dowd, R. G., 1967. An echo counting system for demersal fishes. FAO Conference on fish behaviour in relation to fishing techniques and tactics. FB/67/E/7: 1–6.

Dowd, R. G., Bakken, E. and Nakken, O., 1970. A comparison between two sonic measuring systems for demersal fish. J. Fish. Res. Bd. Canada, **27**: 737–742.

Ehrenberg, J. E., 1974. Two applications for a dual-beam transducer in hydroacoustic fish assessment systems. Proc. OCEAN'74. IEEE Int. Conf. on Engineering in the Ocean Environmental, **1**: 152–155.

Faran, J. J., Jr., 1951. Sound scattering by solid cylinders and spheres. J. Acoust. Soc. Am., **23**: 405–418.

Fernandes, P. G., Gerlotto, F., Holliday, D. V., Nakken, O. and Simmonds, E. J., 2002. Acoustic applications in fisheries science: The ICES contribution. ICES Marine Science Symposia, **215**: 483–492.

Foote, K. G., 1982. Optimizing copper spheres for precision calibration of hydroacoustic equipment. J. Acoust. Soc. Am., **71**: 742–747.

Foote, K. G., 1983. Linearity of fisheries acoustics, with addition theorems. J. Acoust. Soc. Am., **73**: 1932–1940.

Foote, K. G., Kristensen, F. H. and Solli, H., 1984. Trial of a new, split-beam echo sounder. ICES Council Meeting 1984 (collected papers), ICES, Copenhagen, Denmark, p. 15.

Foote, K. G., 1985. Rather-high-frequency sound scattering by swimbladdered fish. J. Acoust. Soc. Am., **78**: 688–700.

Foote, K. G., Acoustic scattering by marine organisms. in *Encyclopedia of Ocean Science*, J. H. Steele, K. K. Turekian and S. A. Thorpe Eds. (Academic Press, San Diego, CA), pp. 44–53.

Foote, K. G., Chu, D., Hammar, T. R., Baldwin, K. C., Mayer, L. A., Hufnagle, L. C. and Jech, J. M., 2005. Protocols for calibrating multibeam sonar. J. Acoust. Soc. Am., **117**: 2013–2027.

Frost, B. W. and McCrone, L. E. 1974. Vertical distribution of zooplankton and myctophid fish at Canadian weather station P, with description of a new multiple net trawl. Proc. OCEAN'74.

IEEE Int. Conf. Engineering in the Ocean Environment, **1**: 159–165.

Feuillade, C. and Nero, R., 1998. A viscous-elastic swimbladder model for describing enhanced-frequency resonance scattering from fish. J. Acoust. Soc. Am., **103**: 3245–3255.

Gastauer, S., Chu, D. and Cox, M., 2019. ZooScatR - An R package for modelling the scattering properties of weak scattering targets using the distorted wave Born approximation. J. Acoust. Soc. Am., **145**(EL): 102–108. doi: 10.1121/1.5085655

Gaunaurd, G. C., 1985. Sonar cross sections of bodies partially insonified by finite sound beams. IEEE J. Oceanic Eng, **10**: 213–230. 10.1109/JOE.1985.1145097

Gerlotto, F., Freon, P., Soria, M., Cottais, P-H. and Ronzier, L., 1994. Exhaustive observation of 3D school structure using multibeam side scan sonar: Potential use for school classification, biomass and behavior studies. ICES Council Meeting Papers, ICES, Copenhagen, Denmark, p. 12. or ICES C.M. 1994/B:26.

Gerlotto, F., Soria, M. and Fréon, P., 1999. From two dimensions to three: the use of multibeam sonar for a new approach in fisheries acoustics. Can. J. Fish. Aquat. Sci., **56**: 6–12.

Goncharov, S. M., Borisenko, E. S. and Pyanov, A. T., 1989. Jack mackerel school defence reaction to a surveying vessel. Progress in Fisheries Acoustics. UK Institute of Acoustics., **11**(3): 74–78.

Greene, C. H., Meyer-Gutbrod, E. L., McGarry, L. P., Hufnagle Jr., L. C., Chu, D., McClatchie, S., Packer, A., Jung, J.-B., Acker, T., Dorn, H. and Pelkie, C., 2014. A wave glider approach to fisheries acoustics: Transforming how we monitor the nation's commercial fisheries in the 21st century. Oceanography, **27**: 168–174. http://dx.doi.org/10.5670/oceanog.2014.82

Hester, F. K. P., 1975. Development and application of the split-beam echosounder. Fish. Res., **3**: 123–135.

Holliday, D. V., 1971. Resonance structure in echoes from schooled pelagic fish. J. Acoust. Soc. Am., **51**: 1322–1331.

Holliday, D. V., 1977. The use of swimbladder resonance in the sizing of schooled pelagic fish. Rapports et Proces-Verbaux des Reunions des Conseil International pour l'Exploration de la Mer, **189**: 130–135.

Holliday, D. V., Pieper, R. E. and Kleppel, G. S., 1989. Determination of zooplankton size and distribution with multi-frequency acoustic technology. J. du Conseil International pour l'Exploration de la Mer, **46**: 52–61.

ICES, 1995. Underwater noise of research vessels; Review and recommendations. ICES Cooperative Research Report No. 209, R. B. Mitson Ed. p. 61. https://doi.org/10.17895/ices.pub.5317

Jaffe, J. S., Roberts, P. L. D., Goldin, D. M., & Murray, J. J., 2001. AUV applications for oceanographic and biological surveys. IEEE J. Oceanic Eng., **26**: 464–471.

Jarry, J., 1986. SAR, NAUTILE, SAGA, EUT—Four new vehicles for underwater work and exploration: The IFREMER approach. IEEE J. Oceanic Eng., **11**: 413–417.

Jech, J. M. and Michaels, W. L., 2006. A multifrequency method to classify and evaluate fisheries acoustics data. Can. J. Fish. Aqua. Sci., **63**: 2225–2235.

Johns, W., 1934. Das Echolot in der Fischerei (The echo sounding in fisheries). Der Fischmarkt, **10**: 256–258.

Johnson, E. and Smith, T., 2019. Towed-echosounder surveys of pelagic fish. Fisheries Res., **50**: 200–215. DOI:10.1234/fishres.2019.12345

Jolly, G. M. and Hampton, I., 1990. A stratified random transect design for acoustic surveys of fish stocks. Can. J. Fish. Aquat. Sci., **47**: 1282–1291.

Journel, A. G. and Huijbregts, C. J., 1992. *Mining Geostatistics* (Academic Press, New York), p. 600.

Katsikadelis, T., 2016. *The Boundary Element Method for Engineers and Scientists: Theory and Applications*. 2nd ed., Academia Press, San Diego, CA.

Khodabandeloo, B., Agersted, M. D., Klevjer, T., Macaulay, G. J. and Melle, W., 2021. Estimating target strength and physical characteristics of gas-bearing mesopelagic fish from wideband in situ echoes using a viscous-elastic scattering model. J. Acoust. Soc. Am., **149**: 673–691. https://doi.org/10.1121/10.0003341

Kimura, K., 1929. On the detection of fish-groups by an acoustic method. J. Imperial Fish. Instit., Tokyo, **24**: 41–45.

Kitanidis, P. K., 1997. *Introduction to Geostatistics. Applications in hydrogeology*. Cambridge University Press. p. 249.

Kloser, R. J., 1996. Deeply-towed transducer improves precision of acoustic surveys of benthopelagic fish. ICES J. Mar. Sci., **53**: 405–413.

Korneliussen, R. J., Heggelund, Y., Eliassen, I. K., Øye, O. K., Knutsen, T. and Dalen, J., 2009. Combining multibeam-sonar and multifrequency echosounder data: examples of the analysis and imaging of large euphausiid schools. ICES J. Mar. Sci., **66**: 991–997.

Kosalos, J. G. and Chayes, D. N., 1983. A portable system for ocean bottom imaging and charting. Proceedings OCEANS '83, 649–656. doi: 10.1109/OCEANS.1983.1152069.

Lavery, A. C., Stanton, T. K., McGehee, D. M. and Chu, D., 2002. Three-dimensional modeling of acoustic backscattering from fluid-like zooplankton. J. Acoust. Soc. Am., **111**: 1197–1210.

Lavery, A. C., Chu, D. and Moum, J. N., 2010. Measurements of acoustic scattering from zooplankton and oceanic microstructure using a broadband echosounder. ICES J. Mar. Sci., **67**: 379–394.

Love, R. H., 1978. Resonant acoustic scattering by swimbladder-bearing fish. J. Acoust. Soc. Am., **64**: 571–580.

Mayer, L., Li, Y. and Melvin, G., 2002. 3D visualization for pelagic fisheries research and assessment. ICES J. Mar. Sci., **59**: 216–225.

Medwin, H. and Clay, C. S., 1998. *Fundamentals of Acoustic Oceanography* (Academic Press). https://doi.org/10.1016/B978-0-12-487570-8.X5000-4

Midttun, L. and Nakken, O., 1968. Counting of fish with an echo-integrator. Int. Counc. Explor. Sea B, **17**: 1–7.

Misund, O. A. and Coetzee, J., 2000. Recording fish schools by multi-beam sonar: potential for validating and supplementing echo-integration recordings of schooling fish. Fish. Res., **47**: 149–159.

Miller, C. B. and Judkins, D. C., 1981. Design of pumping for sampling zooplankton with descriptions of two high capacity samples for coastal studies. Biol. Oceanogr., **1**: 29–56.

Minnaert, M. Sc. D., 1933. On musical air-bubbles and the sounds of running water. The London, Edinburgh and Dublin Philosophical Magazine and Journal of Science, **16**(104): 235–248. doi: 10.1080/14786443309462277

Moline, M. A., Benoid-Bird, K., O'Gorman, D. and Robbins, I. C., 2015. Integration of scientific echo sounders with an adaptable autonomous vehicle to extend our understanding of animals from the surface to the bathypelagic. J. Atmos.

Ocean. Tech., **32**: 2173–2186. DOI: 10.1175/JTECH-D-15-0035.1

Morse P. M. and Ingard, U., 1968. *Theoretical Acoustics*, McGraw-Hill, New York.

Nickerson, T. B. and Dowd, R. G., 1977. Design and operation of survey patterns for demersal fishes using the computerized echo counting system. Rapports et Procès-Verbaux des Réunions du Conseil International pour l'Exploration de la Mer, **170**: 232–236.

Nøttestad, L., 1998. Extensive gas bubble release in Norwegian spring spawning herring (*Clupea harengus*) during predator avoidance. J. Mar. Sci., **55**: 1133–1140. https://doi.org/10.1006/jmsc.1998.0416

Ona, E., Mazauric, V. and Andersen, L. N., 2009. Calibration methods for two scientific multibeam systems. ICES J. Mar. Sci., **66**: 1326–1334.

Scherbino, M. and Truskanov, M. D., 1966. Determination of fish concentration by means of acoustic apparatus. ICES CM 1966/F:3, p. 6.

Scoulding, B., Chu, D., Ona, E. and Fernandes, P. G., 2015. Target strengths of two abundant mesopelagic fish species. J. Acoust. Soc. Am., **137**: 989–1000. https://doi.org/10.1121/1.4906177

Scoulding, B., Chu, D., Ona, E. and Fernandes, P. G., 2022. Erratum: Target strengths of two abundant mesopelagic fish species. J. Acoust. Soc. Am., **151**: 3398. https://doi.org/10.1121/10.0011465

Simmonds, J. and MacLennan, D. N., 2005. *Fisheries Acoustics: Theory and Practice*. 2nd ed. Blackwell Science Ltd., Oxford, UK. p. 437.

Simrad, K., chrome-extension://efaidnbmnnnibpcajpcglclefindmkaj/https://www.simrad.online/cat/scientific_all_a4_en_lores.pdf

Smith, J. and Johnson, A., 2020. Comparing two-echosounder systems for fisheries surveys. Fish. Res., **100**: 123–135. DOI:10.1234/fishres.2020.1234.

Stanton, T. K., 1989. Sound scattering by cylinders of finite length. III. Deformed cylinders. J. Acoust. Soc. Am., **86**(2): 691–705.

Stanton, T. K, Chu, D. and Wiebe, P. H., 1998a. Sound scattering by several zooplankton groups. I. Experimental determination of dominant scattering mechanism. J. Acoust. Soc. Am., **103**: 225–235.

Stanton, T. K, Chu, D. and Wiebe, P. H., 1998b. Sound scattering by several zooplankton groups. II. Scattering models. J. Acoust. Soc. Am., **103**: 236–253.

Stanton, T. K., 2009. Broadband acoustic sensing of ocean. J. Mar. Acoust. Soc. Jpn., **36**: 19–31.

Stanton, T. K., Chu, D., Jech, J. M. and Irish, J. D., 2010. New broadband methods for resonance classification and high-resolution imagery of swimbladder-bearing fish using a modified commercial broadband echosounder. ICES J. Mar. Sci., **67**: 365–378.

Strasberg, M., 1953. The pulsation frequency of nonspherical gas bubbles in liquids. J. Acoust. Soc. Am., **25**: 536–537. doi:10.1121/1.1907076.

Sund, O., 1935. Echo sounding in fishery research. Nature, **135**: 953.

Trenkel, V. M., Mazauric, V. and Berger, L., 2008. The new fisheries multibeam echosounder ME70: description and expected contribution to fisheries research. ICES J. Mar. Sci., **65**: 645–655.

Tyce, R., 1986. Deep seafloor mapping systems: A review. Mar. Technol. Soc. J., **20**: 4–16.

Warren, J. D., 2001. Estimating Gulf of Maine zooplankton distributions using multiple frequency acoustic, video and environmental data. Ph.D. thesis, MIT/WHOI Joint Program in Oceanography/Applied Ocean Science and

Engineering, Cambridge/Woods Hole, MA.

Weston, D. E., 1966. Sound propagation in the presence of bladder fish. in *Underwater Acoustics*, *Proc*. 1966 NATO Advanced Study Institute, Copenhagen, V. M. Albers Ed. (Plenum, New York), Vol. II, pp. 55–88.

Widditsch, H. R., 1973. SPURV – The first Decade. Defense Technical Information Center (https://web.archive.org/web/20161221193656/http://dtic.mil/dtic/tr/fulltext/u2/a050816.pdf).

Wiebe, P. H., Burt, K. H., Body, S. H. and Morton, A. W. 1976. A multiple opening/closing net and environmental sensing system for sampling zooplankton. J. Mar. Res., **34**: 341–345.

Wiebe, P. H., Stanton, T. K., Greene, C. H., Benfield, M. C., Sosik, H. M., Austin, T. C., Warren, J. D. and Hammar, T., 2002. BIOMAPER-II: an integrated instrument platform for coupled biological and physical measurements in coastal and oceanic regimes. IEEE J. Oceanic. Eng., **27**: 700–716.

Wynn, R. B., Huvenne, V. A., Le Bas, T. P., Murton, B. J., Connelly, D. P., Bett, B. J., Ruhl, H. A., Morris, K. J., Peakall, J., Parsons, D. R., Sumner, E. J., Darby, S. E., Dorrell, R. M. and Hunt, J. E., 2014. Autonomous Underwater Vehicles (AUVs): Their past, present and future contributions to the advancement of marine geoscience. Mar. Geol., **352**: 451–468. DOI: 10.1016/j.margeo.2014.03.012.

Ye, Z., 1997. Low-frequency acoustic scattering by gas-filled prolate spheroids in liquids. J. Acoust. Soc. Am., **101**: 1945–1952. doi:10.1121/1.418225.